Journal of Membrane Science 628 (2021) 119226

Contents lists available at ScienceDirect

Journal of Membrane Science

journal homepage: http://www.elsevier.com/locate/memsci

Towards a systematic determination of multicomponent gas separation with membranes: the case of CO_2/CH_4 in cellulose acetates

Eleonora Ricci [a,d,*], Ernesto Di Maio [b], Micaela Degli Esposti [a,d], Liang Liu [c], Giuseppe Mensitieri [b], Paola Fabbri [a,d], Sandra E. Kentish [c], Maria Grazia De Angelis [a,d,e]

[a] Department of Civil, Chemical, Environmental and Materials Engineering, University of Bologna, Via Terracini 28, 40131, Bologna, Italy
[b] Dipartimento di Ingegneria Chimica, dei Materiali e della Produzione industriale, University of Naples, P.le Tecchio, 80, Naples, Italy
[c] School of Chemical and Biomedical Engineering, University of Melbourne, Parkville, VIC, 3010, Australia
[d] Consorzio Interuniversitario di Scienza e Tecnologia dei Materiali (INSTM), Via Giusti 9, 50121, Firenze, Italy
[e] Institute for Materials and Processes, School of Engineering, University of Edinburgh, Sanderson Building, Robert Stevenson Road, EH9 3FB, Scotland, UK

ARTICLE INFO

Keywords:
Mixed gas transport
CO_2/CH_4 separation
Semicrystalline polymers
NELF model
ST model

ABSTRACT

This work aims at obtaining a systematic description and prediction of the multicomponent gas separation behavior of membranes, using the Non-Equilibrium Lattice Fluid (NELF) model for gas sorption and the Standard Transport (ST) model for gas permeation. The scheme is applied to a comprehensive analysis of CO_2/CH_4 separation with cellulose acetate membranes. A dedicated experimental campaign (pressure-volume-temperature (*PVT*), differential scanning calorimetry (DSC) and pure gas sorption tests) was performed to obtain reliable model parameters, accounting also for crystallinity. The approach was validated against a complete set of literature data, including mixed gas sorption and permeation.

The parameters obtained were used to perform predictive simulations of mixed CO_2/CH_4 sorption and permeation in a wide mixture composition range. The NELF model accurately predicts the effect of temperature on sorption, as well as the strong competitive exclusion of CH_4 when CO_2 is present, that enhances the solubility-selectivity. The ST model correctly estimates the experimentally observed lower-than-ideal CO_2/CH_4 perm-selectivity. The model shows that low perm-selectivity is due to mixed gas diffusivity-selectivity (which is not available experimentally): even though solubility-selectivity increases in the mixed gas case, diffusivity-selectivity suffers a larger departure from pure gas conditions, ultimately leading to a lower perm-selectivity under multicomponent conditions.

1. Introduction

In the design of gas separation processes it is important to assess the membrane performance under mixed gas conditions, because multicomponent phenomena can greatly affect the separation, especially in the presence of highly sorbing gases like CO_2. Indeed, the available experimental mixed gas sorption and permeation results in glassy polymers for gas separations [1–14] reveal that the presence of a highly sorbing component in the feed stream induces a significant decrease in the solubility of the less soluble species, but at the same time promotes their faster diffusion, due to the increased swelling associated to highly sorbing penetrants. The balance of such effects has to be considered for the proper evaluation of membrane selectivity.

The number of experimental data of mixed gas permeability and more recently, also solubility and diffusivity, has increased, especially for the CO_2/CH_4 mixture. Therefore, it is now possible to develop and validate a systematic modelling approach that can address and explain the effects observed in multicomponent sorption and transport, enabling the design and optimization of membrane separation processes. A good simulation strategy for multicomponent separation in polymeric membranes should be based on models for sorption and transport that are reliable in the multicomponent case, with accurate model parameters, and should be validated on the largest possible set of experimental data.

In this work, we devise a comprehensive modelling approach, that addresses both multicomponent sorption and permeation of the CO_2/CH_4 mixture in a commercially relevant polymeric membrane based on Cellulose Acetates (CAs) [15]. Cellulose acetates have held a long-standing presence in the field of membrane separations, being

* Corresponding author. Department of Civil, Chemical, Environmental and Materials Engineering, University of Bologna, Via Terracini 28, 40131, Bologna, Italy.
E-mail address: eleonora.ricci12@unibo.it (E. Ricci).

https://doi.org/10.1016/j.memsci.2021.119226
Received 5 November 2020; Received in revised form 28 January 2021; Accepted 23 February 2021
Available online 17 March 2021

traditionally employed in the industry for water desalination with reverse osmosis [16,17] and for natural gas sweetening [18,19]. Indeed, cellulose triacetate (CTA) was the first material in use for removal of CO_2 and H_2S from natural gas, and it remains among the few polymers commercialized to date for use in industrial CO_2/CH_4 separation [20]. In addition, the research interest in CAs as a membrane material is still very high, for natural gas and biogas treatment [21], as well as for post-combustion CO_2 capture [22], due to their good CO_2/N_2 and CO_2/H_2 selectivity and commercial readiness.

Despite being widely employed in membrane separations and thoroughly characterized experimentally, they are relatively less studied from the modelling point of view. The simulation of CAs is difficult due to their complex nature: at room conditions they are found in semi-crystalline morphology with amorphous domains in the glassy state, with properties depending on the degree of acetylation or degree of substitution (DS) [23], a parameter which indicates the average number of acetate groups per glucose unit. The different steric hindrance and electronegativity of hydroxyl (HO-) and acetate (CH_3COO-) groups results in different chain packing efficiency and mobility, which ultimately affects the volumetric, mechanical and gas transport properties. In particular, factors such as the density, crystallinity, thermal properties, but also the gas solubility and permeability are a function of the DS of the material, as well as of the fabrication conditions [23–26].

Among the very few modelling studies found in the literature regarding CAs, Saberi et al. [27,28] proposed a permeation model based on the Dual Mode Sorption (DMS) model for solubility and on the partial immobilization model for diffusivity, whose adjustable parameters are obtained through fitting of experimental mixed gas data. Unlike the framework presented in this work, the work from Saberi and co-workers lacks predictive character for the mixed-gas case, since a different set of parameters is used at each mixture composition analyzed, preventing exploration of conditions outside those included in the fitting set. Magnanelli et al. [29] developed a model to represent CO_2/CH_4 permeation through asymmetric cellulose acetate, including both the effects of heat and mass transport. For the description of solubility in the dense selective layer they employed the empirical DMS model and neglected the presence of other impurities in the stream. Guo et al. [30,31] proposed a modified DMS model accounting for hole formation to address inconsistencies found in the application of the traditional DMS model to sorption-desorption hysteresis curves. Perrin et al. modelled water and ethanol sorption in CA using the Engaged Species Induced Clustering (ENSIC) model to account for clustering of the penetrant molecules [32]. These analyses share a common trait: they adopted an empirical representation of gas solubility, through the DMS model. This model provides a very good fitting of pure gas data, but it does not provide a good representation in the case of mixed gas sorption [33], therefore it was not adopted in this work.

Instead, the Non-Equilibrium Lattice Fluid (NELF) model [34] for mixed gas sorption and the Standard Transport (ST) model [35] for multicomponent transport were selected for this work, due to their ability to describe complex polymeric structures and multicomponent effects. This selection accounts for the development of a modular approach, since the two models are linked through Solution-Diffusion theory [36]. The model enables the reliable calculation of n-component mixed gas sorption using only pure and binary mixture parameters [8]. We use it as a module of the ST model for permeability, and also in a stand-alone fashion, to predict multicomponent sorption for comparison with experimental data. Dedicated experimental tests of the volumetric and calorimetric behavior of CDA and CTA allowed us to obtain the pure polymer model parameters, while binary energetic and swelling parameters were obtained on pure gas sorption measurements in the same materials. The sorption model and parameters thus obtained were validated against pure gas solubilities at different temperatures and mixed gas solubilities recently published [5]. The simulation of mixed gas permeation was performed with the multicomponent version of the ST model proposed by Minelli and Sarti [37], that estimates the permeability, according to the Solution-Diffusion model, as the product of solubility (calculated with the NELF model) and diffusivity [35]. The diffusivity is estimated as the product of a kinetic factor named the mobility coefficient, which is adjusted based on pure gas permeability data; and a thermodynamic factor which is again evaluated using the Non-Equilibrium approach. The model can perform predictive evaluations of multicomponent permeability, with no additional parameters with respect to the pure gas permeation case [37]. The calculation of binary CO_2/CH_4 permeation with the model was validated in this work against literature data for CTA and CDA.

The separate analysis of multicomponent gas sorption and diffusion effects is particularly useful because the experimental characterization of mixed gas diffusion is extremely difficult, while this property has a tremendous impact on the separation behavior of glassy polymeric membranes. The combination of model parametrization, validation and simulation will demonstrate the capability of the proposed systematic strategy to model mixed gas transport in these materials of great industrial relevance and leverage the theoretical framework to gain a deeper understanding of the separation phenomena.

2. Theoretical background

2.1. Solution-diffusion model

The transport of gas molecules in dense polymeric membranes is described by the solution-diffusion model [36]: gas permeability (P) is the product of a thermodynamic factor, the solubility coefficient (S), and a kinetic factor, the diffusion coefficient (D).

$$P = S \cdot D \quad \text{Eq. (1)}$$

Assuming that the downstream pressure is negligibly small, the selectivity of the membrane α_{ij}, which is equal to the ratio between the permeability of the two gases, becomes the product of a solubility-selectivity $\alpha^S_{i,j}$ and a diffusivity-selectivity factor $\alpha^D_{i,j}$:

$$\alpha_{i,j} = \frac{P_i}{P_j} = \frac{S_i}{S_j}\cdot\frac{D_i}{D_j} = \alpha^S_{i,j}\cdot\alpha^D_{i,j} \quad \text{Eq. (2)}$$

In the context of mixed gas sorption experiments and modelling, results are computed and reported using gas fugacity (f) instead of partial pressure, in order to account for the various degrees of non-ideality of the different species. Permeability and solubility coefficients are also defined on a fugacity basis:

$$S_i = \frac{c_i}{f_i} \quad \text{Eq. (3)}$$

$$P_i = \frac{J_i\, l}{f_i^{u} - f_i^{d}} \quad \text{Eq. (4)}$$

c_i is the sorbed concentration of component i, J_i is the steady-state flux of species i, l the membrane thickness, while f_i^{u} and f_i^{d} represent the upstream and downstream fugacity of component i, respectively. Gas fugacity at the various pressures and mixture compositions studied was calculated with the Peng-Robinson equation of state [38], for the sake of convenience. For mixture calculations the following binary interaction parameter was used [39]: $k_{CO_2/CH_4} = 0.09$. The following paragraphs describe the thermodynamic model used to calculate gas sorption and the transport model implemented for the description of permeability.

2.2. Thermodynamic model for solubility

In this work, gas sorption is modelled using the Non-Equilibrium Thermodynamics for Glassy Polymers (NET-GP) approach [34], which is a thermodynamic-based framework that provides the extension of equation of state (EoS) theories to non-equilibrium materials. NET-GP applies to homogeneous, isotropic, and amorphous phases, whose

state is described by the usual set of state variables, namely temperature T, pressure p and composition Ω, and, in addition, by the non-equilibrium density of the glassy polymer ρ_{pol}, which acts as an internal state variable and accounts for all the effects of thermal history and formation of the polymer, responsible for its departure from equilibrium.

The NET-GP approach [40] provides expressions for the chemical potential in non-equilibrium systems, such as glassy polymers, which are derived from the expression for the free energy provided by any EoS of choice. The non-equilibrium chemical potential can then be employed to solve the phase equilibrium for the composition and calculate the solubility in glassy polymers. Even though glassy polymers are not in a thermodynamic equilibrium state, because they tend to densify over time, the dynamics of this process is slow compared to the characteristic time of a sorption process. Therefore, it is possible to assume that a "pseudo" phase equilibrium condition can be reached by the polymer in contact with the gas phase and so calculate the amount of sorbed gas by imposing the equality of the chemical potential of the penetrant i in the two phases:

$$\mu_i^{NE(pol)}\left(T,p,\Omega,\rho_{pol}\right)=\mu_i^{Eq(gas)}\left(T,p,y_i\right) \quad \text{Eq. (5)}$$

In this work we used the Non-Equilibrium Lattice Fluid (NELF) version of the NET-GP approach [34,41], which is an extension of the Sanchez-Lacombe (SL) equation of state [42,43]. A detailed list of all the variables and symbols pertaining to the SL and NELF models is reported in Appendix A. Additional details can be found in these reference works [40,44].

In the SL EoS and NELF model, each pure component is described by three parameters, T^*, p^*, and ρ^*. These parameters are obtained by fitting the SL EoS to pressure-volume-temperature (PVT) data above the glass transition temperature (T_g), in the equilibrium region of the material:

$$\tilde{\rho}=1-\exp\left[-\frac{\tilde{\rho}^2}{\tilde{T}}-\frac{\tilde{p}}{\tilde{T}}-\tilde{\rho}\left(1-\sum_i^N\frac{\varphi_i}{r_i}\right)\right] \quad \text{Eq. (6)}$$

The SL and NELF models share also an adjustable gas-polymer binary interaction parameter k_{ij}, which can be obtained by fitting the SL or the NELF model to sorption isotherms, above or below T_g, respectively. In the case of gas mixtures, binary parameters for gas-gas interactions should also be introduced. However, previous works [13] have shown that these binary parameters have a negligible effect on mixed gas sorption calculations, therefore they can be set equal to zero without compromising accuracy.

Non-equilibrium calculations differ from equilibrium ones, because knowledge of the polymer density ρ_{pol} is required as input for non-equilibrium models, while it is calculated by the EoS for equilibrium models, using Eq. (6). Since the polymer density changes along the sorption isotherm, as a result of penetrant sorption, the introduction of a swelling coefficient k_{sw} accounts for its variation in non-equilibrium calculations, in the absence of dilation measurements. A simple linear relationship with penetrant fugacity (f_i) is assumed, which has been found to yield accurate results in previous work [40,44]:

$$\frac{1}{\rho_{pol}}=\frac{1}{\rho_{pol}^0}\left(1+\sum_{i=1}^{N_p}k_{sw,i}f_i\right) \quad \text{Eq. (7)}$$

ρ_{pol}^0 is the dry polymer density, N_p the number of gas species present in the mixture. For each gas-polymer pair, the value k_{sw} is obtained through the best-fit of a pure gas sorption isotherm.

The expression of the chemical potential of the SL model, to be used to solve the phase equilibrium and calculate solubility, is given below:

$$\frac{\mu_i}{RT}=\ln(\tilde{\rho}\varphi_i)-\ln(1-\tilde{\rho})\left[r_i^0+\frac{r_i-r_i^0}{\tilde{\rho}}\right]-r_i-\tilde{\rho}\frac{r_i^0v_i^*}{RT}\left[p_i^*+\sum_{j=1}^{N}\varphi_i\left(p_j^*-\Delta p_{i,j}^*\right)\right]+1 \quad \text{Eq. (8)}$$

It is noteworthy that, in the case of mixed gas sorption, only pure component parameters and binary parameters obtained from pure gas data are necessary. Therefore, sorption calculations for gas mixtures can be performed predictively, once the pure gas measurements are available.

One of the major obstacles in modelling CA membranes with the aforesaid model is the presence of crystallites. Indeed, even though semi-crystalline polymers are widely used in several relevant applications, the rigorous modelling of their sorption and transport behavior is still a debated issue. The NELF model allows only for the simulation of sorption in the amorphous phase of a semi-crystalline structure, considered as homogenous and isotropic. The crystalline phase is generally considered inert and not contributing to the sorption of fluids. In recent years, some more sophisticated approaches have tried to account for the effect of the crystalline domains on the sorption properties of the amorphous phase, allowing a more accurate description of the process. Such studies were developed and validated only on materials in which the amorphous phase is rubbery, *i.e.* above their glass transition. In particular, Bonavoglia et al. [45] argued that the presence of the crystalline phase hinders the mobility of the amorphous rubbery one, to a point that it behaves like a non-equilibrium one. Thus, sorption in the amorphous phase is calculated with a non-equilibrium model and an adjusted value of the density. Minelli and De Angelis [46] and more recently, Fischlschweiger et al. [47] also considered the rubbery amorphous phase to be constrained by the presence of crystallites, but instead of invoking a non-equilibrium behavior, considered that the amorphous phase is at equilibrium with a much higher pressure value than the one imposed by the gas phase only, due to the stress exerted by the crystals. The total pressure acting on the amorphous phase is the sum of the actual gas pressure and the "constraining pressure" imposed by crystals. The constraining pressure is univocally related to the increased density of the amorphous phase at each value of crystalline fraction, which can be calculated with an equation of state. Unfortunately, the above-mentioned approaches, developed for semicrystalline rubbers, cannot be applied to case of cellulose acetates, which are below their glass transition in the conditions of interest. Therefore, in this study, the crystallites were assumed to be impermeable to gases, while amorphous regions were modelled with the SL and NELF model above and below T_g, respectively. The effect of crystallites is taken into account in the calculation of the density of the amorphous phase, using the experimental volumetric data and the procedure described in Section 3.

2.3. Standard transport model for permeability

The standard transport model implemented in this work [35,37] considers the diffusion coefficient D_i as the product of two factors, a concentration-dependent mobility coefficient L_i and a thermodynamic factor α, which accounts for the dependence of the chemical potential of the gas on its concentration. The multicomponent extension of the model is derived from a generalized Fick's law [48,49], and considers as driving force for isothermal diffusion the negative chemical potential gradient [50]. For each component i present in the mixture (gas or polymer), a corresponding driving force d_i for diffusion is defined [51]:

$$d_i=-\rho\omega_i\nabla\left(\frac{\mu_i}{RT}\right)_{T,P} \quad \text{Eq. (9)}$$

where ρ is the mixture density and ω_i the mass fraction of solute i in the mixture. The constitutive equations for isothermal diffusive fluxes J_i of the n components present in the mixture are defined as follows:

$$J_i = \sum_k^n L_{ik} d_k \quad i = 1 \ldots n \qquad \text{Eq. (10)}$$

L_{ik} is the mobility coefficient of penetrant i in the mixture. The driving forces must satisfy the Gibbs-Duhem equation, therefore $0 = \sum_k^n d_k$. In the case of dilute solutions, such as the case of light gases in a polymer phase, the chemical potential of the polymer can be considered uniform, therefore its gradient negligible: $d_{pol} \approx 0$. Moreover, since the gases are highly diluted in the polymer phase, the mutual interaction between the penetrants can also be neglected: $L_{ik} \approx 0$ if $i \neq k$. In the case of multicomponent solubility calculations it has been previously verified that specific gas-gas interactions are indeed negligible [13]. L_{ii} will be hereafter referred to as L_i for simplicity. Therefore, the set of equations Eq. (10) simplifies to:

$$J_i = -\rho L_i \omega_i \nabla \left(\frac{\mu_i}{RT}\right)_{T,P} \quad i = 1 \ldots n-1 \qquad \text{Eq. (11)}$$

In the case of a ternary system comprised of a mixture of two gases and a polymer the equations describing gas transport in the system become:

$$\begin{cases} J_1 = -\rho L_1 \left(\alpha_{11}\dfrac{\partial \omega_1}{\partial x} + \alpha_{12}\dfrac{\partial \omega_2}{\partial x}\right) \\ J_2 = -\rho L_2 \left(\alpha_{21}\dfrac{\partial \omega_1}{\partial x} + \alpha_{22}\dfrac{\partial \omega_2}{\partial x}\right) \\ x = 0 \ : \ \omega_1 = \omega_1^{\mathrm{u}} \ , \ \omega_2 = \omega_2^{\mathrm{u}} \\ x = l \ : \ \omega_1 = \omega_1^{\mathrm{d}} \ , \ \omega_2 = \omega_2^{\mathrm{d}} \end{cases} \qquad \text{Eq. (12)}$$

The terms α_{ij} are thermodynamic factors defined by the following relation:

$$\alpha_{ij} = \omega_i \frac{\partial(\mu_i/RT)}{\partial \omega_j} \qquad \text{Eq. (13)}$$

The thermodynamic factors describe the relationship between the concentration of the penetrants in the polymer and their chemical potential, thus they are related to the sorption isotherms. Therefore, they can be determined by means of the NELF model, which is used to calculate also the concentration of both gases at the boundaries ω_1^{u}, ω_1^{d}, ω_2^{u}, ω_2^{d} (u = upstream, d = downstream), once the values of the pressure and composition of the gas phase at the two sides of the membrane have been set. From the solution of the set of equations Eq. (12), the molar fluxes of penetrants 1 and 2 are obtained. The corresponding permeability values are then calculated using Eq. (4).

The mobility coefficients L_1 and L_2 are concentration dependent and they change due to swelling induced by penetrant sorption. In the case of single gas transport, an exponential relationship with concentration yields an effective representation [35,52,53] of the experimental data. For the case of binary gas mixtures, to account for the dependency on both concentration values, the following mixing rule is adopted:

$$\begin{aligned} L_1 &= L_1^0 \exp(\beta_{11}\omega_1 + \beta_{12}\omega_2) \\ L_2 &= L_2^0 \exp(\beta_{21}\omega_1 + \beta_{22}\omega_2) \end{aligned} \qquad \text{Eq. (14)}$$

The terms β_{ij} are the plasticization factors in the mixture case, describing how penetrant j affects the permeability of penetrant i. Under the assumption that the mobility dependence on composition for each component is related to the dilation of the polymer matrix induced by it, one can assume $\beta_{11} = \beta_{21} = \beta_1$ and $\beta_{22} = \beta_{12} = \beta_2$. In particular, β_1 and β_2 are the plasticization factors associated to pure gas permeation and can be obtained, together with the infinite dilution mobility coefficients L_1^0 and L_2^0, from the analysis of pure gas permeation curves. This is equivalent to assuming that the extent of plasticization induced by a component is the same in pure and mixed gas conditions, which is consistent with the assumptions made concerning swelling in the thermodynamic model.

3. Experimental methods

3.1. Sample preparation

Cellulose diacetate (CDA), purchased in powder form from Eastman (DS 2.4), and cellulose triacetate (CTA), purchased in pellets form from Acros Organics (DS 2.9), were used in this study.

Thick samples for *PVT* measurements were prepared via solution casting. In the case of CDA, a well stirred 8 wt% solution with acetone was cast into a 7.6 cm Teflon Petri dish and covered to allow for a slow evaporation of the solvent, to obtain a homogeneous and smooth surface of the sample. For CTA, a 5 wt% solution with dichloromethane was prepared, left under magnetic stirring overnight and then cast into a 7.6 cm Teflon Petri dish, which was covered to allow for a slow solvent evaporation. After 12 days at room temperature, the samples, that had detached from the Teflon container and slightly shrunk in diameter, were placed under vacuum at 100 °C for 72 h to remove residual solvent. A final thickness of approximately 1 mm was achieved in both cases.

Films for sorption measurements were obtained using the following protocol. A 5 wt% solution was prepared by dissolving the polymer into dichloromethane (CTA) or acetone (CDA). The solutions were filtered and cast into glass Petri dishes, which were then kept covered for solvent evaporation. After 24 h, the membranes were peeled from the petri dishes and annealed in a vacuum oven for 24 h at 35 °C and another 24 h at 100 °C. The annealed membranes were kept in a desiccator for 14 days prior to utilization in sorption and permeation studies, to minimize the impact of the initial physical aging of the glassy membranes. A final thickness of approximately 50 μm was achieved in both cases.

3.2. Characterization

3.2.1. DSC and TGA measurements

Thermal behavior of the CAs was evaluated by differential scanning calorimetry (DSC) on a Q10 (TA Instruments) equipped with a Discovery Refrigerated Cooling System (RCS90, TA Instruments). Measurements were performed under dry nitrogen flow (50 cm^3/min) on samples of approximately 10 mg placed in an aluminum pan. Samples were analyzed by applying a thermal cycle from 25 to 260 (CDA) and to 320 (CTA) °C, with a heating and cooling rate of 10 and 20 °C/min, respectively. Three independent tests were performed for each material. Before the measurements, the system was calibrated both in temperature and enthalpy with an Indium standard. The weight loss decomposition profiles were investigated by thermogravimetric analysis (TGA, Q50, TA Instruments) under dry nitrogen flow (60 cm^3/min) on samples of about 20 mg placed in platinum pans. Samples were heated from room temperature to 450 °C with a rate of 10 °C/min. Peak temperatures of thermal degradation (T_{deg}) were determined as the temperatures corresponding to the maximum of the thermogravimetric derivative (DTG) curves. Both DSC and TGA thermograms were processed with TA Universal Analysis 2000.

3.2.2. Room temperature density and *PVT* measurements

Pressure-volume-temperature (*PVT*) measurements were performed using a GNOMIX high pressure dilatomer (Boulder, CO, USA). This apparatus is based on a well-established bellow technique, in which a hydrostatic pressure is applied to a sample of the investigated material, whose volume is known at reference values of pressure and temperature. The material is surrounded by mercury as confining, pressure transmitting fluid. The volume change in the measuring cell filled with mercury and the sample is evaluated by a linear variable differential transducer mounted beneath the pressure vessel. The corresponding actual volume change of the sample, induced by the applied pressure, is calculated after subtraction of the volume change of the confining fluid (mercury) from the total volume of the cell. The measurement procedure

is described in detail elsewhere [54].

The apparatus is able to collect data in the range from 10 to 200 MPa in increments of 10 MPa, and from room temperature up to 400 °C. The tests were carried out using an isothermal compression procedure in the range 30–220 °C for CTA and 30–250 °C for CDA, at 10 °C intervals, and from 10 to 200 MPa, at 10 MPa intervals. The choice of an isothermal mode of measurement rather than an isobaric one is dictated by the necessity to reduce the thermal degradation of the samples. However, the specific volume data above T_g, which are the ones of interest in this work, are not affected by the specific thermodynamic path followed, but they depend only on the actual pressure and temperature values at which they were measured.

By using this dilatometric technique, one is able to perform only measurements of volume change, therefore the value of the volume of the polymer sample at known pressure and temperature conditions (reference values of P and T) must be provided as input, to evaluate the absolute values of the sample volume in the whole range. First, the values of volume change at the reference P (atmospheric pressure) were estimated using the Tait equation [55], by extrapolating the values of the volume change from 30 MPa to 10 MPa at several temperatures. From these values, the value of volume change at the reference temperature was obtained (this is an automated procedure performed using the internal GNOMIX software). Finally, by comparing this value with the volume of the sample at reference conditions, the entire set of data was rescaled, transforming volume changes into absolute values of volume. The value of the volume of the samples of CDA and CTA at the reference P and T values was obtained from the density measurements by means of the buoyancy method, using hexane as displacement fluid [56].

3.2.3. Pure gas sorption measurements

The single gas sorption measurement was conducted in a Gravimetric Sorption analyser (BELSORP). Each sample (*i.e.* CTA or CDA) was pre-treated at 35 °C under vacuum (<0.001 Pa) for 10 h. Then CH_4 or CO_2 was introduced in a stepwise manner from 100 to 4000 kPa and the quantity absorbed was measured by a Magnetic Suspension Balance (Rubotherm, MSB). The sorption equilibrium at each pressure was monitored by a mass change rate of less than 0.002 mg over 2 min.

4. Results

4.1. Models parametrization

4.1.1. Calorimetric tests and determination of crystallinity

It is well known that the thermal behavior of CAs varies depending on the cellulose source, which impacts on molecular weight and polydispersity, and the method and degree of acetylation [25,57,58]. Based on this observation, DSC analysis was performed on real samples taken from the specimens prepared for *PVT* measurements. This test allows the estimation of the crystalline fraction, required for the calculation of the density of the amorphous phase of the polymer, as indicated in Eq. (16). DSC curves are displayed in Fig. 1 and in Fig. S1 in the Supporting Information.

The crystalline fraction of the samples was calculated through the following relation:

$$\text{crystalline fraction}\ (\text{wt}\%) = \frac{\Delta H_m - \Delta H_{cc}}{\Delta H_m^o} \cdot 100 \qquad \text{Eq. (15)}$$

where ΔH_m and ΔH_{cc} are the enthalpies of melting and cold crystallization (observed for CTA only) and ΔH_m^0 is the enthalpy of melting for the 100% crystalline CTA, whose value was taken to be 58.8 J/g [59]. In the absence of specific data, the same value of the enthalpy of melting was applied also to CDA [24,60]. The measured crystalline fractions are 31% ± 2 and 51% ± 2 for CDA and CTA, respectively, and are consistent with literature evidence [24,61]. Standard deviations are obtained from the average of three tests.

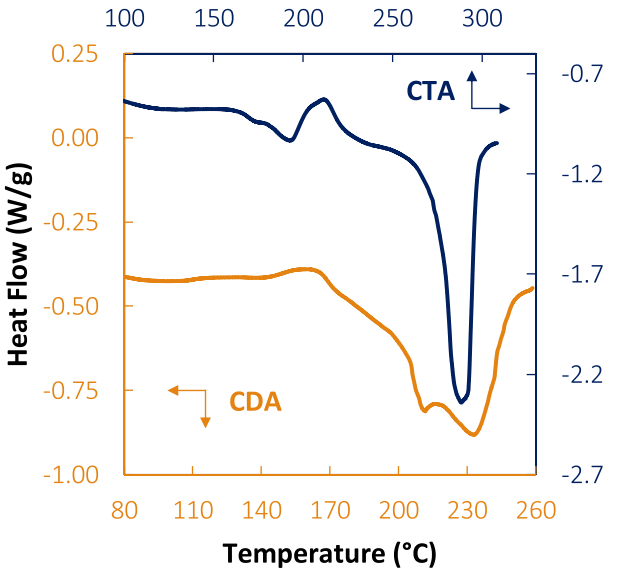

Fig. 1. Representative DSC thermograms for CDA (orange, read on lower and left axis) and CTA (blue, read on upper and right axis), magnified in the regions of recorded transitions and recorded during the first heating scan. Exothermic transitions are displayed by positive peaks in DSC curves. (For interpretation of the references to color in this figure legend, the reader is referred to the Web version of this article.)

The melting behavior of CDA confirms complex transitions with a broad melting peak spread over the range 210–250 °C, with two different endothermic peaks at about 210 °C and 230 °C, consistently with literature data [62]. CTA exhibits a sharp melting peak centered at 288–290 °C and an exothermic peak related to cold crystallization at 211–213 °C observed in the heating scan, confirming literature data [25]. The crystal structure of CAs is rather complex and has been studied in several works [63–68], also with the support of molecular modelling analysis [69,70]. Two distinct polymorphs, CTA I and CTA II, have been traditionally observed, with parallel [63] and antiparallel [64] chain arrangement, respectively. More recently, a third structure, named CTA III, has been observed in partially acetylated materials [71], which presents differences in its structural and thermal characteristics and lower stability compared to CTA I. A detailed characterization of the crystal phase composition in terms of different polymorphs was beyond the purposes of the present work, and the simplifying assumption of a uniform crystal structure was adopted.

By the observation of DSC curves, T_g can also be detected. For CTA we observed a complex endothermic baseline shift between 165 and 185 °C, which can be ascribed to the relaxation of amorphous domains accordingly to the reported literature [25]. On the contrary, a T_g partially overlapped to the onset of the melting transition was observed for CDA at about 160–167 °C. Previous studies [25] suggested an increasing trend of T_g with decreasing DS, while the two samples used in this work exhibited similar values. Several factors may affect the thermal behavior of the different types of CAs, and considering that the objective of the present analysis was not to perform a detailed investigation of the thermal properties of the samples, but rather to provide guidelines for subsequent tests, this aspect was not investigated further.

The thermal stability of CAs in the temperature range investigated during the *PVT* tests was confirmed by TGA analysis. Weight loss decomposition profiles displayed in Fig. S1 in the Supporting Information, are consistent with data previously reported in the literature [23–25,57,58]. In particular, TGA plots show a main weight loss with T_{deg} extrapolated from DTG at 365 and 368 °C for CTA and CDA, respectively, corresponding to the main thermal degradation of polymer chains. Another small weight loss (5–6%) can be observed from room

temperature to the onset of the main degradation, due to the volatilization of the volatile matter, and/or the evaporation of small amount of residual absorbed water [24,72]. The charred residue (16 and 13% for CTA and CDA, respectively) at 450 °C in nitrogen atmosphere is consistent with previously reported data [23,72,73].

4.1.2. Determination of SL EoS pure polymer parameters on PVT data

The densities of the samples at 25 °C were measured with the buoyancy technique, as explained in Section 3.2.2, and are reported in Table 1. The measurement was repeated 5 times for each sample, showing high repeatability. Lower density values for higher DS samples are consistent with observations in the literature [74].

The results of *PVT* tests performed on CDA and CTA samples are shown in Fig. 2. Only five curves per sample are shown, for clarity. The data set is reported in full in the Supporting Information in Table S1 and Table S2. In Fig. 2, data to the right of the dashed lines constitutes the rubbery region of the material [75], that is the one of interest in the evaluation of the SL EoS parameters.

No melting occurred during the tests, which would be visible as a step-like increase in the specific volume as temperature increases [75]. Thermal expansion coefficients at atmospheric pressure were evaluated and are reported in Table 2: higher values were obtained for CDA, both in the glassy and rubbery state. An estimate of the glass transition temperature from the curves at atmospheric pressure is presented and discussed in the Supporting Information (Fig. S2)

The density of the amorphous fraction of the samples, ρ_A, is used to estimate the SL parameters for the polymers. Such values can be obtained from the above reported data of experimental density of the semi-crystalline material, ρ_{SC}, assuming volume additivity between the amorphous and crystalline phases, that results in the following relation:

$$\rho_A = \frac{\rho_C(1-\omega_C)}{\frac{\rho_C}{\rho_{SC}} - \omega_C} \qquad \text{Eq. (16)}$$

where ω_C is the weight fraction of the crystallites, obtained from DSC analysis and ρ_C the crystal density. Since no melting was observed in the temperature range inspected during the *PVT* test, the crystalline fraction is assumed to be constant in the whole dataset. From the observation of the T_m values extrapolated from DSC tests, we were expecting to observe the melting of CDA. However, due to the different conditions of the two tests, melting was not observed in the *PVT* experiment. The value 1.375 g/cm^3 [65] is used for ρ_C at room temperature, the value 15.6×10^{-5} K^{-1} [76] for the volumetric thermal expansion coefficient of the CTA I crystal. A typical value of 1×10^{-4} MPa^{-1} [77,78] for the isothermal compressibility coefficient of polymeric crystals is used, in the absence of a specific measurement for CTA I. The coefficients were assumed to be constant in the whole temperature and pressure range, consistent with the fact that the crystalline fraction remains unvaried until the melting conditions are reached.

It must be pointed out that the above procedure allows for a realistic evaluation of the amorphous phase density in the presence of crystallites, i.e. in its constrained state, which is the one actually encountered during membrane operations.

The amorphous dry polymer density at 25 °C for CDA is equal to 1.277 g/cm^3, while 1.212 g/cm^3 was calculated for CTA. These data can be compared with the results of atomistic simulations on amorphous cellulose acetate performed by Bocahut et al. [79], that report a density of 1.22 g/cm^3 and 1.19 g/cm^3 for CDA and CTA respectively. The higher density of amorphous CDA displayed both by experiments and simulations can be explained by the lower number of acetate substituents, which are bulkier than the hydroxyl groups. The difference of 4% in the case of CDA and 2% in the case of CTA of the experimental density values compared to the simulated ones can be a result of the constraining effect exerted by the crystalline fraction on the amorphous one in our samples, which leads to higher values for the amorphous density and which is absent in molecular simulations, that consider a hypothetical unconstrained amorphous phase. As mentioned above, the procedure used in this paper provides a value of the amorphous density that is more realistic, as the materials used for separation are actually semi-crystalline and the amorphous phases in which the gases permeate are found in a constrained state.

Table 1
Density of the samples used in *PVT* and sorption measurements.

	CDA	CTA
$\rho_{25\,°C}$– thick samples (g/cm^3)	1.300 ± 0.5%	1.281 ± 0.5%
$\rho_{25\,°C}$ – thin samples (g/cm^3)	1.306 ± 0.5%	1.290 ± 0.5%

By fitting the resulting data of the amorphous phase to the Sanchez-Lacombe equation of state, parameters for CDA and CTA were retrieved. In Fig. 3 the results of the fitting procedure are shown, with dashed lines delimiting the glassy and rubbery region as described previously. The best fit parameters obtained for each material are summarized in Table 3. 95% confidence intervals, which account for parameter coupling, were obtained with a Monte Carlo method [80]. As can be seen, the model is able to capture the volumetric behavior of cellulose acetate accurately. Some deviation is seen in the case of CTA at the lower pressures in proximity of the glass transition, which is probably related to the fact that the material showed a broad region of transition in slope, rather than a marked and well-defined discontinuity. Agreement with points at higher temperature, which are more likely to belong to the true equilibrium region of the material, provides a more conclusive validation of the results.

4.1.3. Determination of binary NELF model parameters on pure gas sorption isotherms

Pure CO_2 and CH_4 sorption isotherms in CDA and CTA were measured at 35 °C and the results are shown in Fig. 4. Moreover, in Fig. S3 in the Supporting Information, the results are compared with the measurements of Puleo et al. [24], finding very good agreement with the literature values. Concentrations are compared in Fig. S3 also rescaling the values by dividing them by the amorphous phase weight fraction $(1-\omega_c)$, since it was assumed in the modelling that the gas is present only in the amorphous phase. When the different crystallinity of the samples is taken into account (37 wt% for CDA and 52 wt% for CTA in the data from the literature [24]) the curves obtained here overlap with the literature ones.

The ability of the cellulose acetate SL parameter sets reported in Table 3 to represent gas sorption in the glassy state was tested by modelling CO_2 and CH_4 sorption data at 35 °C for CDA and CTA using the NELF model. The corresponding values of the dry amorphous polymer densities at 35 °C were calculated using the thermal expansion coefficient of the amorphous phase determined for each material from the experimental *PVT* measurements.

The concentration expressed with respect to amorphous polymer mass was considered in the analysis with the NELF model. The values of the best fit binary interaction parameters and swelling coefficients obtained are reported in Table 4. The model was able to give a faithful representation of the experimental data with low values of the binary interaction coefficients. It can be noted that the swelling coefficient obtained for CO_2 sorption in CTA is double than the value obtained for CDA. In the case of CH_4 very small values of the swelling coefficients were obtained as best fit parameters. This value is often assumed to be zero, when sorption at lower pressure (around 3 MPa) is calculated with the NELF model [40]. However, the present data set extends well beyond 3 MPa, therefore dilation effects are no longer negligible. The values of k_{sw} obtained for both CDA and CTA are similar for this gas.

4.1.4. Determination of ST model binary parameters on pure gas permeation data

In order to evaluate the parameters needed to describe the mobility of gases using the standard transport model, pure gas permeability data

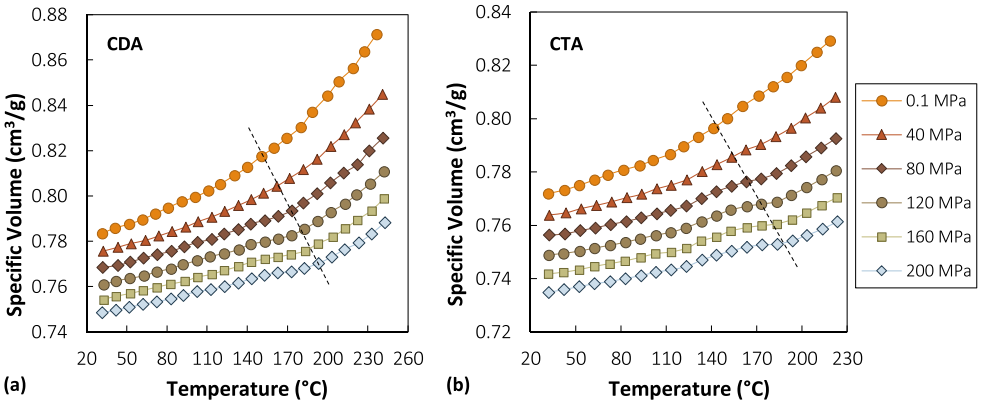

Fig. 2. *PVT* curves for CDA (a) and CTA (b).

Table 2
Thermal expansion coefficients of semicrystalline CDA and CTA at atmospheric pressure.

	Glass	Rubber
CDA	$2.9 \cdot 10^{-4}$ K^{-1}	$8.1 \cdot 10^{-4}$ K^{-1}
CTA	$2.4 \cdot 10^{-4}$ K^{-1}	$5.8 \cdot 10^{-4}$ K^{-1}

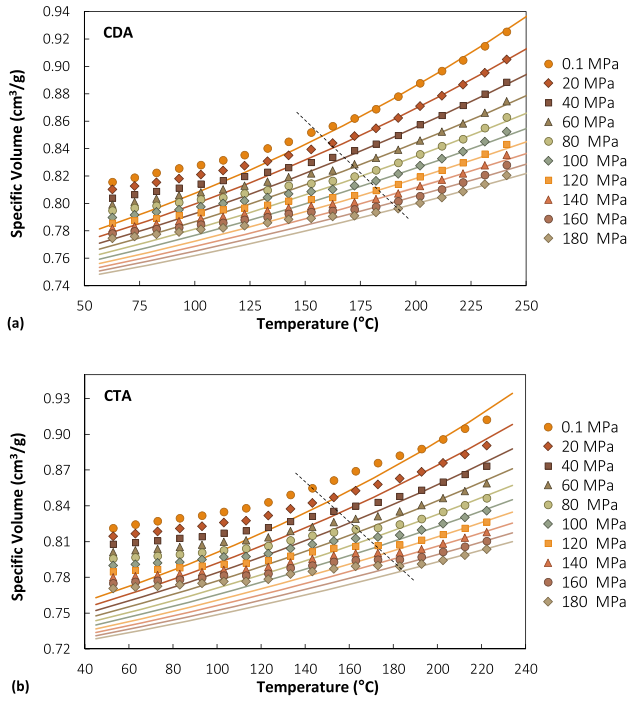

Fig. 3. *PVT* data of the amorphous fraction of CDA (a) and CTA (b), together with Sanchez Lacombe EoS calculations performed with the parameters reported in Table 3.

Table 3
SL parameters for amorphous CDA and CTA.

	CDA	CTA
T* (K)	608 ± 8	560 ± 6
P* (MPa)	730 ± 15	780 ± 20
ρ* (g/cm^3)	1.400 ± 0.005	1.450 ± 0.005

from the literature are considered [81,82]. The values of infinite dilution mobility coefficient and plasticization factor obtained are reported in Table 5. The NELF parameters for pure polymers (Table 3) and the binary coefficients (Table 4) retrieved in this work were employed to calculate the thermodynamic factors. The crystalline fraction of the material was assumed to be impermeable to gases, consistent with the assumption made in sorption modelling. It should be noted the impermeability of the crystallites would reflect in a longer diffusive path for the penetrant molecules. In this work a tortuosity factor was not introduced to take this effect into account, as it would increase the number of adjustable parameters required by the analysis. Rather, this effect is implicitly included in the effective values of the mobility coefficients determined from the best fit of pure gas permeability data. In the case of CH_4, the concentration dependence of the mobility factor, expressed by β, is negligible, consistently with the very low dilation induced by the gas to the polymer. The results of the calculations are shown in Fig. 5. In the case of CTA, the model is able to well represent both pure gas permeability curves, with a maximum 16% deviation in the case of CO_2 at high pressure. In the case of CDA, the representation of the data is highly accurate in the case of CH_4 in the whole pressure range and in the case of CO_2 up to 3 MPa, whereas at higher pressure significant underestimation occurs.

The sensitivity of the results to the values of the adjustable parameters was explored both for solubility and permeability calculations, considering CO_2 in CTA as an example, and the results are shown in Fig. S5 of the Supporting Information. A 10% variation of the parameters was tested, and it was observed that in the case of k_{ij} this had a negligible effect on the calculated results, in the case of k_{sw} the effect is negligible at low pressure and more pronounced at high pressure, with a maximum deviation at 4 MPa of 9% compared to the reference case. In the case of the variation of L_0 the results show a uniform 10% variation in the whole range, while in the case of β the effect is negligible at low pressure and more pronounced at higher pressure, with a maximum deviation at 2.5 MPa of 5% compared to the reference case.

4.2. Model validation and predictive simulations

4.2.1. Validation of the NELF model and CDA parameters for pure gas sorption at various temperatures

As a test of consistency and transferability of the SL parameters obtained for CDA, two literature data sets were analyzed [83,84], which report the solubility of CH_4 and CO_2 as a function of temperature. In neither of these works a measurement of the crystalline content of the film is reported, therefore the value of the amorphous density of our CDA samples was assumed. The temperature dependence of the density was accounted for using the thermal expansion coefficient at atmospheric pressure retrieved from the *PVT* measurements.

The data set was well represented by the NELF model, as can be seen

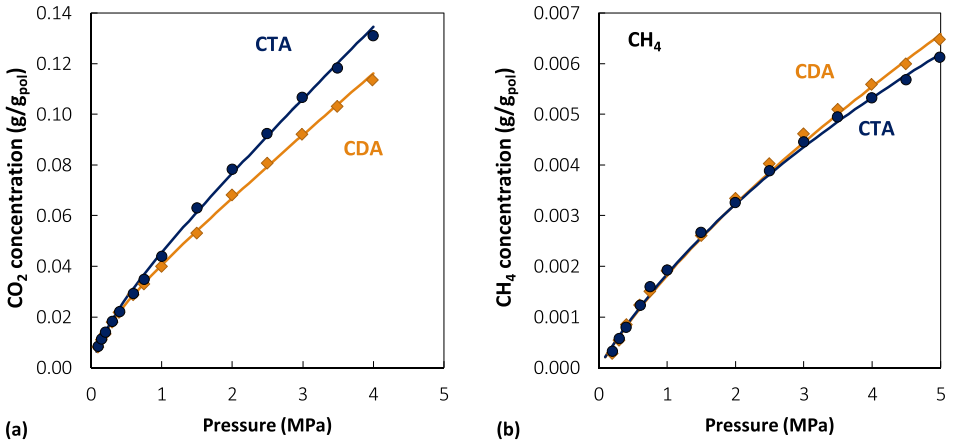

Fig. 4. Sorption isotherms of (a) CO_2 and (b) CH_4 in CTA (blue circles) and CDA (orange diamonds) at 35 °C. Lines represent NELF model calculations. (For interpretation of the references to color in this figure legend, the reader is referred to the Web version of this article.)

Table 4
Binary parameters of the NELF model for gas-polymer systems at 35 °C.

	$k_{CO_2,pol}$	k_{sw,CO_2} (MPa^{-1})	$k_{CH_4,pol}$	k_{sw,CH_4} (MPa^{-1})
CDA	−0.070	0.037	−0.098	0.004
CTA	0.021	0.061	0.024	0.003

Table 5
ST model parameters used to calculate CO_2 and CH_4 permeability in CTA.

	CTA		CDA	
	L^0 (cm^2/s)	β	L^0 (cm^2/s)	β
CO_2	$1.1 \cdot 10^{-8}$	5	$2.9 \cdot 10^{-9}$	10.5
CH_4	$5.3 \cdot 10^{-9}$	0	$1.4 \cdot 10^{-9}$	0

in Fig. 6. Notably, the best fit values of the parameters obtained (reported in Table 6) are highly consistent with those determined for our samples (reported in Table 4). The binary interaction parameters were constant in the case of CO_2, coinciding with the value reported in Table 4. The values of k_{ij} for CH_4 obeyed a weak linear temperature dependence, which yields the same value reported in Table 4 for our samples if extrapolated to 35 °C. The swelling coefficients were found to follow a quadratic temperature dependence. k_{sw} approaches zero at 30 °C in the case of CH_4, which is consistent with the low value obtained at 35 °C reported in Table 4. These temperature dependencies are quite common when exploring data at different temperatures [8,85,86]. A 34% difference in the swelling coefficient of CO_2 was obtained, compared to the value regressed over our sorption isotherm. Such differences in the values of the swelling coefficients can likely be ascribed to the uncertainty in the crystalline fraction of literature data, that reflects on the density values used in the calculation, which affect greatly the calculated solubility.

On the whole, the pure component SL parameters for CDA obtained in this work from *PVT* data describe well the literature sorption data for CO_2 and CH_4 at different temperatures, demonstrating generality and transferability within a broad range of operating conditions.

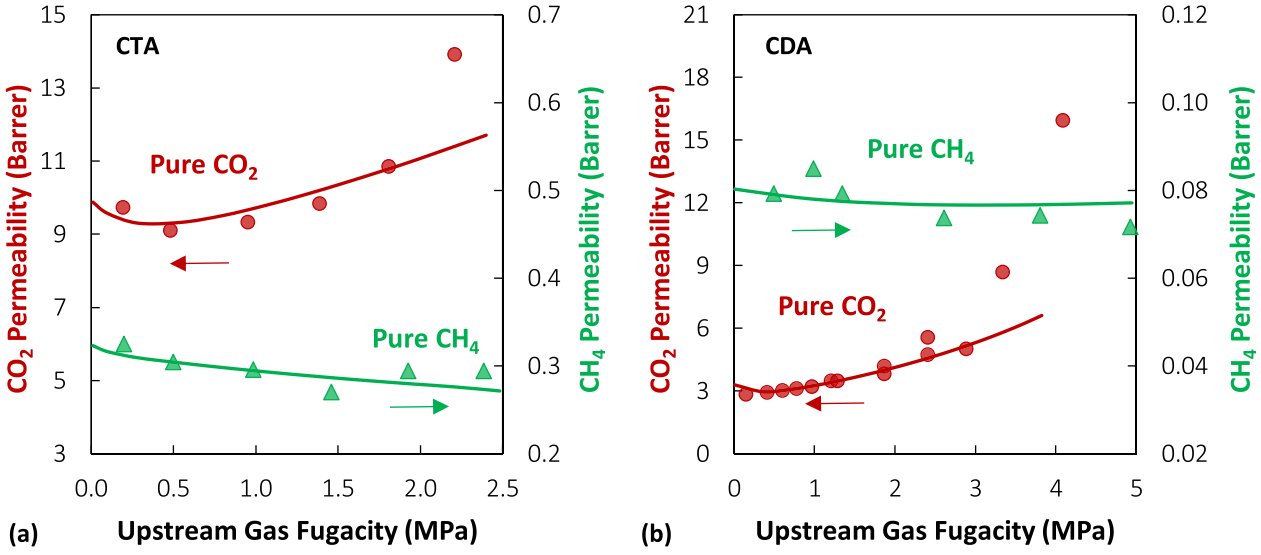

Fig. 5. Pure gas permeability of CO_2 (red) and CH_4 (green) in (a) CTA and CDA (b) at 35 °C. Experimental data from Refs. [81,82]: filled symbols represent pure gas data, lines represent ST model predictions. (For interpretation of the references to color in this figure legend, the reader is referred to the Web version of this article.)

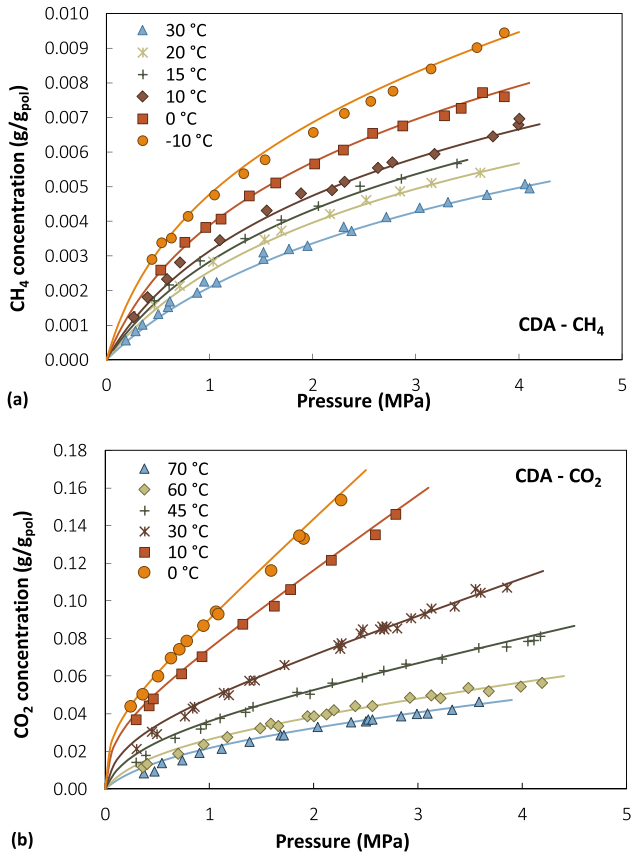

Fig. 6. Experimental sorption isotherms of (a) CH_4 (ref. [84]) and (b) CO_2 (ref. [83]) in cellulose diacetate at different temperatures, together with NELF model calculations.

Table 6
Temperature dependence of the binary interaction and swelling coefficients used to model sorption isotherms of CO_2 and CH_4 in CDA from Refs. [83,84].

	k_{ij} (T in K)	k_{sw} MPa^{-1} (T in K)
CH_4	$-5.31 \cdot 10^{-4}\,T + 6.54 \cdot 10^{-2}$	$1.59 \cdot 10^{-6}\,T^2 - 9.62 \cdot 10^{-4}\,T + 0.14$
CO_2	$-7.00 \cdot 10^{-2}$	$1.33 \cdot 10^{-5}\,T^2 - 9.10 \cdot 10^{-3}\,T + 1.57$

4.2.2. Validation of the NELF model and CTA parameters on mixed gas sorption data

Measurements of mixed gas sorption of CO_2/CH_4 mixtures in CTA at 35 °C were recently reported [5], which can be used to validate the proposed approach and CTA parameters. Pure gas sorption isotherms of CO_2 and CH_4 measured by Genduso and coworkers coincide with those by Puleo et al. [24] as do ours (Fig. S3), consequently the parameters reported in Tables 1 and 4 are expected to be appropriate also for their data. The results are shown in Fig. 7. The experimental results are obtained at a different equilibrium mixture composition in each case. In the graph we grouped by color and symbol type the results obtained at a similar mixture composition, to facilitate an understanding of the results. However, the different individual values of the equilibrium gas mixture composition of each mixed gas sorption experiment were taken into account in the calculation. The individual composition of each point is reported in Table S4 in the Supporting Information, together with experimental measurements and NELF model predictions.

Good agreement can be observed across the whole data set. The average relative difference (absolute value) between model results and experiments is 8% in the case of CO_2, while it increases to 22% in the case of CH_4, however, this is within the experimental uncertainty of the data, as can be seen in Fig. 8. These results provide a positive indication of the transferability also of the CTA pure polymer parameters, and validation of the adopted procedure for the calculation of pure and mixed gas sorption in cellulose acetates using the NET-GP framework.

4.2.3. Validation of the ST model and CTA, CDA parameters on mixed gas permeation data

The set of parameters obtained by fitting pure gas permeation data to the ST model (Table 6) was employed to perform a predictive simulation of the permeation of an equimolar CO_2/CH_4 mixture, comparing the results with the measurements from Ref. [81] in Fig. 8a. Good agreement is observed between the experimental data and model predictions for both gases. The maximum deviation is observed at the highest pressure and amounts to a 36% underestimate for both gases.

In Fig. 8b, the perm-selectivity of CTA is displayed and compared with ST model calculations. The trends are well captured by the model, both at ideal and multicomponent conditions. The diffusivity-selectivity, which is not available experimentally, can be evaluated by means of the ST model. As can be seen in Fig. 8, while the mixed gas value of α_S is on average 1.8 times higher than the ideal value calculated from pure gas values, the diffusivity-selectivity α_D exhibits the opposite behavior, with multicomponent values equal to about 1/3 of the pure gas ones. The diffusivity is thus the factor quantitatively more affected by multicomponent effects and leads to a calculated mixed gas perm-selectivity on average equal to 64% of the pure gas value, in line with the experimental

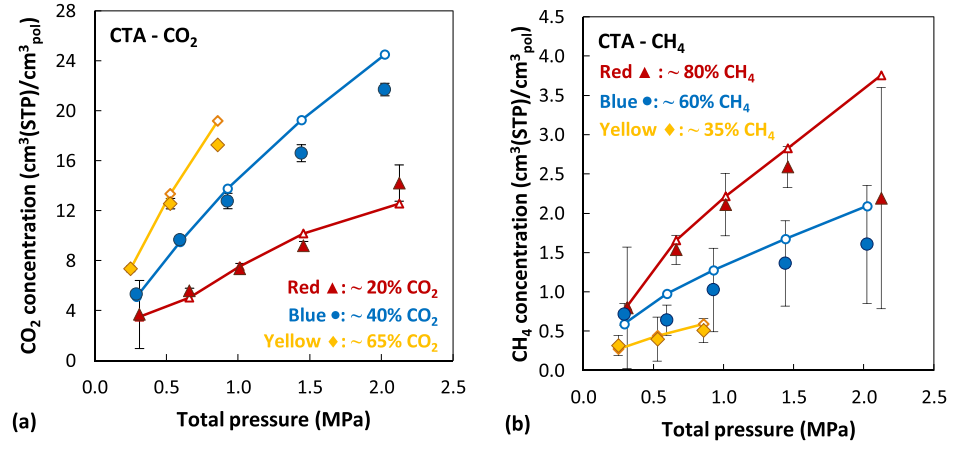

Fig. 7. Mixed gas sorption of CO_2 and CH_4 in CTA. Filled symbols: experimental data from Ref. [5]. Empty symbols with solid lines: NELF model predictions. Colors and symbols represent data at similar mixture composition to facilitate the visualization, however each point was calculated at its corresponding equilibrium composition, reported in the original reference and also in Table S4 for convenience. (For interpretation of the references to color in this figure legend, the reader is referred to the Web version of this article.)

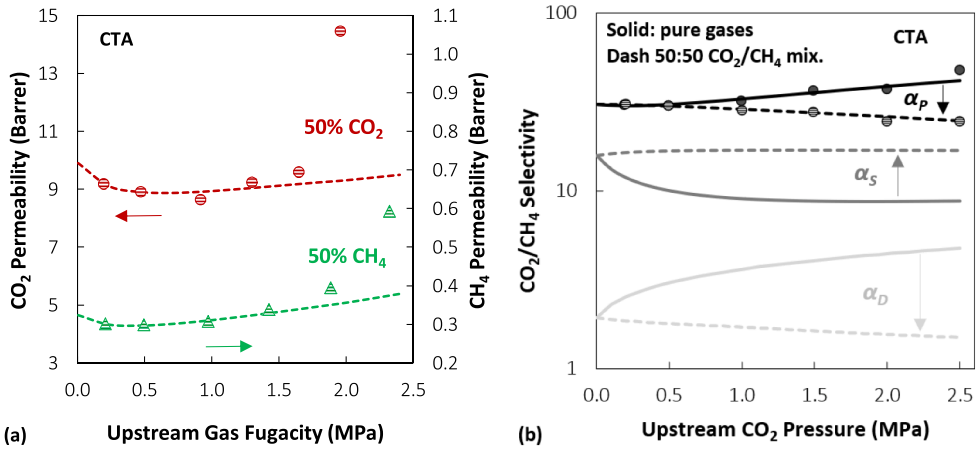

Fig. 8. (a) Permeability of CO_2 (red) and CH_4 (green) in CTA at 35 °C. Experimental data from Ref. [81]: symbols represent mixed gas data at equimolar composition. Dashed lines represent ST model predictions. (b) Perm-selectivity (black), solubility- (gray) and diffusivity-selectivity (light gray) of CO_2/CH_4 at ideal conditions (solid lines) and for an equimolar mixture (dashed) predicted by the ST model. Symbols are experimental perm-selectivity from Ref. [81]. (For interpretation of the references to color in this figure legend, the reader is referred to the Web version of this article.)

data. Comprehensive analysis of the available literature have shown that this trend is obeyed by all glassy polymers for which mixed gas permeation and sorption data are available [5,13] and it was shown here that it can be reliably reproduced and predicted by means of the ST model applied in the NET-GP framework.

An analogous analysis of mixed gas CO_2/CH_4 permeability in CDA at three different mixture compositions is reported in Fig. 9. The agreement with the experimental data of mixed gas permeability available [82] is lower than in the case of CTA, especially in the low pressure and high CO_2 composition range. However, we believe that this discrepancy could be attributed to the generally higher error associated with the measurement of CH_4 permeability. Indeed, its values are significantly lower in CDA than in CTA (~0.1 Barrer) and may be close to the resolution limit of the instruments (the y-axis in Fig. 9b spans just 0.5 Barrer). Moreover, one can notice from the Figure that the CH_4 permeability data at different compositions do not collapse to one single curve when the pressure approaches zero, as predicted by the model and confirmed by the CTA permeability trend. Furthermore, an intrinsically higher uncertainty of CH_4 permeability data is confirmed by the fact that different sources have documented different values for CH_4 pure and mixed gas permeability in CDA, as can be seen in Fig. 9b, with the multicomponent values either increasing or decreasing compared to the pure gas case. Therefore, in the case of CDA, the comparison with available experimental data does not offer conclusive grounds to validate the model.

4.2.4. *Predictive simulation of CO_2/CH_4 mixed gas sorption, diffusion and permeation in CDA and CTA with the combined modelling approach*

Having validated the model parameters using mixed gas sorption and permeation data, a systematic predictive analysis of the effect of mixture composition and pressure on mixed gas solubility, diffusivity and permeability was carried out. Indeed, the NELF and ST models allow mixed gas sorption and permeation calculations to be performed predictively, using the parameters of the pure components and those of the binary pure gas-polymer systems, which can be used to expand the mixed gas behavior information in a wider range than the one explored experimentally.

Three different compositions of the CO_2/CH_4 mixture (10/90–30/70–50/50 CO_2/CH_4 mol%) in CDA and CTA at 35 °C were simulated and the results in terms of mixed gas solubility, diffusivity, permeability as well as the corresponding selectivities are reported in Fig. 10, Fig. 11, Fig. 12, Fig. 13. A total pressure range up to 5 MPa was explored.

The results of NELF predictions of CO_2/CH_4 mixtures solubility for the three compositions analyzed are shown in Fig. 10. Data are reported in terms of gas fugacity. Strong competitive sorption effects are displayed by both materials: CH_4 sorption is markedly lowered in the presence of CO_2, while at multicomponent conditions CO_2 is sorbed to a very similar extent to the pure gas case. Indeed, the experimental data also confirms an average 2% decrease in sorbed concentration compared to the pure gas case for CO_2 [5]. For CAs the difference in solubility of CO_2 and CH_4 is remarkably high, almost an order of magnitude, which can explain why CO_2 is less affected by competition compared to other glassy polymers: previous analysis [1] had shown that the higher the

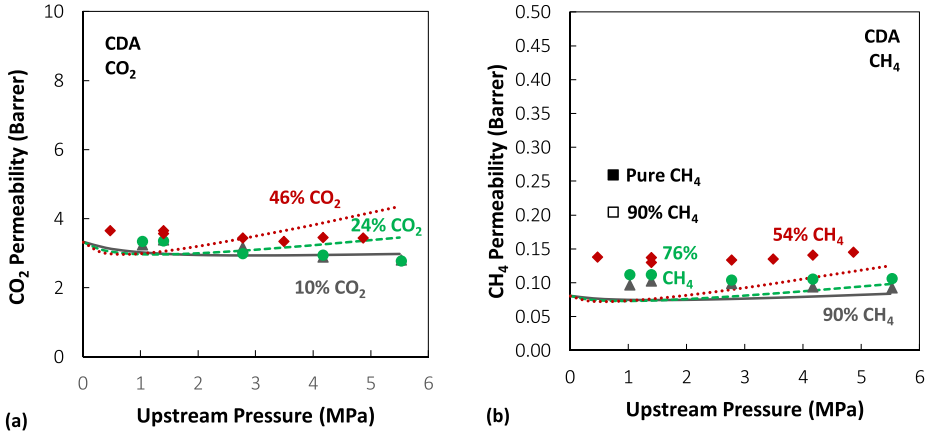

Fig. 9. Permeability of CO_2 (a) and CH_4 (b) in CDA at 35 °C. Experimental data from Ref. [82] are shown: red diamonds 46% CO_2-54% CH_4 mixture, green circles 24% CO_2-76% CH_4 mixture, gray triangles 10% CO_2-90% CH_4 mixture. Mixed gas data for CH_4 pure and mixed gas permeation from Ref. [61] are shown with squares in (b) for comparison, to exemplify the variability in CH_4 permeability. Lines represent ST model predictions: solid 10% CO_2, dash 24% CO_2, dot 46% CO_2. (For interpretation of the references to color in this figure legend, the reader is referred to the Web version of this article.)

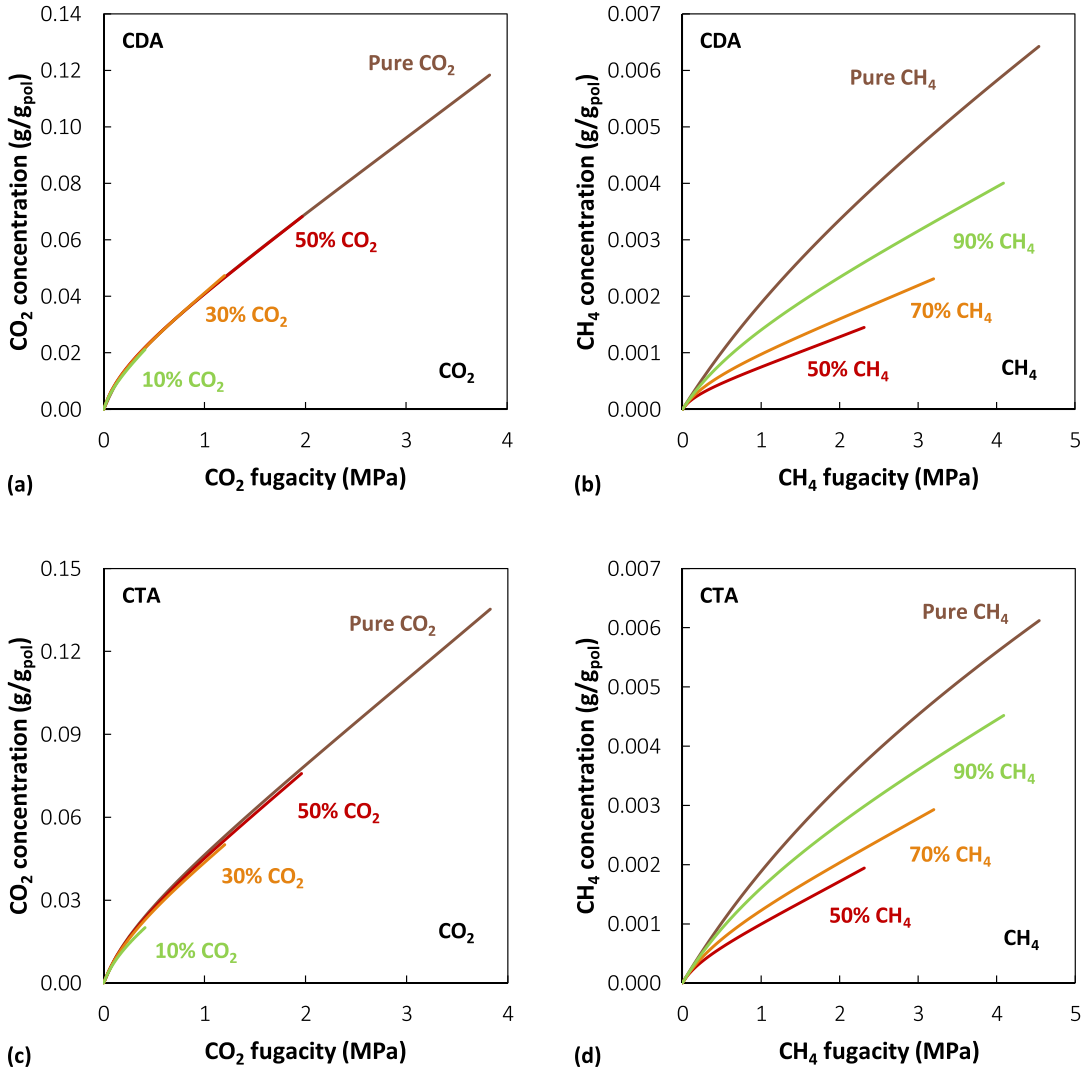

Fig. 10. Mixed gas sorption of 10/90 (green), 30/70 (orange) and 50/50 (red) mol% CO_2/CH_4 mixtures in CTA and CDA at 35 °C calculated with the NELF model. The brown lines represent pure gas sorption. (For interpretation of the references to color in this figure legend, the reader is referred to the Web version of this article.)

molar concentration of one gas with respect to another inside the membrane, the more favored it would be in the competition for sorption sites.

Fig. 11 shows the diffusion coefficients calculated with the ST model for CO_2 and CH_4 in CDA and CTA. It is clearly appreciable how strongly the presence of CO_2 in the mixture promotes a faster CH_4 diffusion, owing to swelling effects, whereas CO_2 values remain close to pure gas conditions. In the case of CDA, mixed gas diffusion coefficients have a stronger concentration dependence, consistently with the higher value of the parameter β (Table 6).

The CO_2/CH_4 mixed gas permeability in CDA and CTA at 35 °C was calculated at the same values of mixture composition, and the results are reported in Fig. 12. It is worth noting that in the case of mixed-gas permeability, the model predictions were affected by a larger deviation at high pressure, compared to the case of mixed-gas sorption results. Nonetheless, a consistent picture emerges from the data and the analysis of the concentration trends. Results are reported in terms of gas fugacity in the upstream side. In both CDA and CTA, at low fugacity values the permeability of CH_4 decreases as the amount of CO_2 in the gas phase is increased, which is a direct consequence of competitive sorption effects. On the other hand, at high fugacity values the trend is reversed and CH_4 permeability increases when more CO_2 is present in the mixture, which can be attributed to CO_2-induced swelling effects. Interestingly, in the case of CO_2 permeability in CDA, the mixture composition does not appear to have any effect, while in the case of CTA, CO_2 permeability decreases as the concentration of CO_2 in the gas phase decreases. This can be related to a decrease in solubility rather than diffusivity, as can be seen by comparing the solubility and diffusivity coefficients of CO_2 in CDA and CTA, reported in Fig. S3 and Fig. 11 respectively.

The presence of minima in the calculated permeability curves is not to be attributed to the presence of a so-called plasticization pressure for the material, but it is rather associated to the interplay of the trends of solubility and diffusivity contributions with increasing pressure. Solubility coefficient values (Fig. S3) decrease with increasing pressure, while diffusion coefficients always increase (Fig. 11). For each mixture composition, the relative magnitude of these two factors will determine the overall trend of the permeability curve.

The effects of competitive sorption on solubility-, diffusivity- and perm-selectivity are shown in Fig. 13. In the same Figure, the corresponding values of the ideal selectivity at all compositions are shown

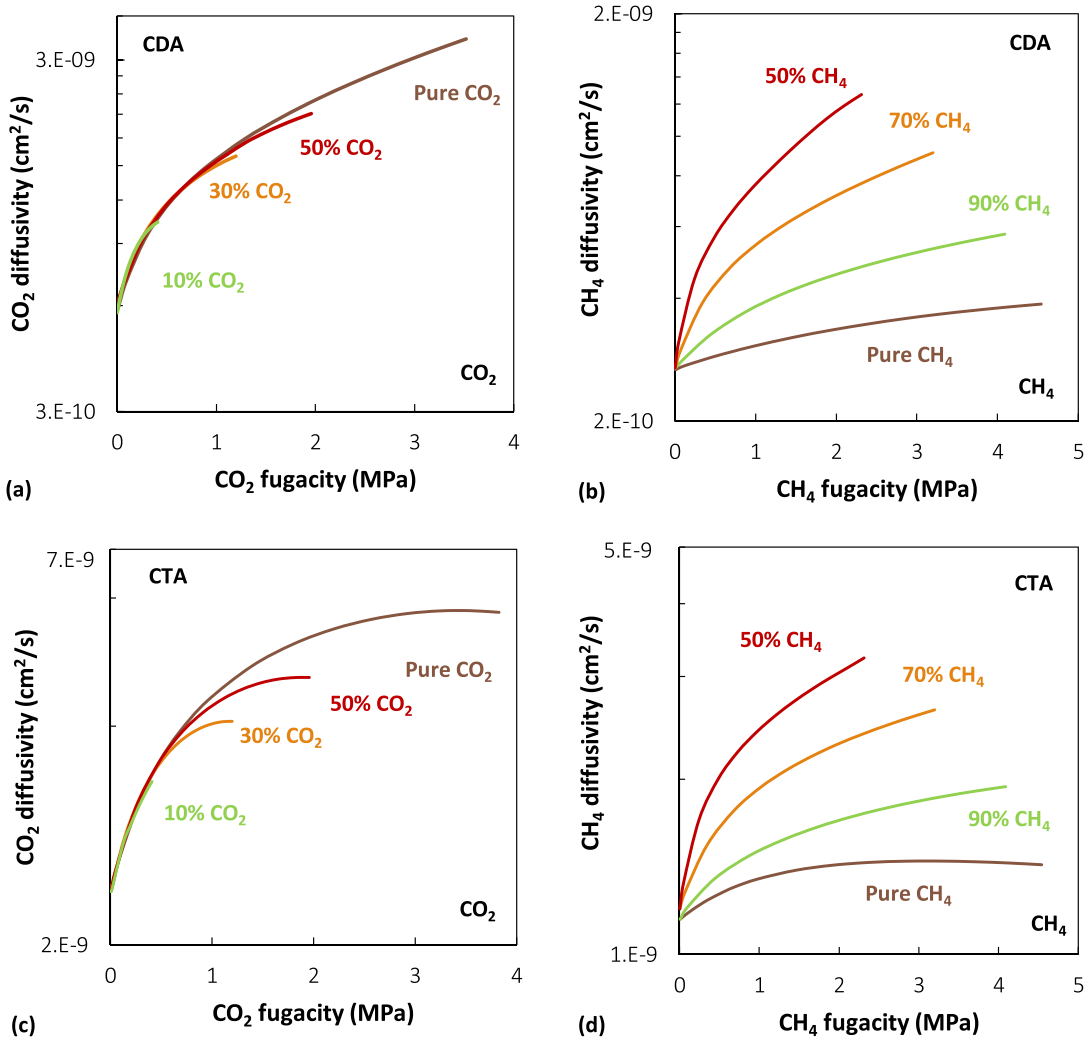

Fig. 11. Mixed gas diffusion coefficients of 10/90 (green), 30/70 (orange) and 50/50 (red) mol% CO_2/CH_4 mixtures in CTA and CDA at 35 °C calculated from the solution-diffusion relation. The brown lines represent pure gas diffusion coefficients. (For interpretation of the references to color in this figure legend, the reader is referred to the Web version of this article.)

and compared. The latter are calculated using the pure gas concentration/diffusion/permeability values corresponding to the fugacity that the gas has in the mixture case. Therefore, the comparison between the pure and mixed gas case is performed at constant fugacity of the gas. Solubility was calculated on a molar basis.

It is striking to notice the difference between the limited concentration dependence of solubility-selectivity and the very broad variation with composition of ideal selectivity calculations. This result demonstrates the inaccuracy that is present in this kind of estimates when mixture effects, such as competitive sorption, are neglected. The uncertainty in the solubility-selectivity calculation was assessed as reported in the Supplementary Information (Fig. S4): the variability associated to the uncertainty in the SL parameters is limited (about ±2.5%), which is an indication of the robustness of the model.

Diffusivity- and perm-selectivity values are shown in Fig. 13 as well. The diffusivity-selectivity follows the opposite trend with respect to ideal values, compared to solubility-selectivity: it is lower at multicomponent conditions and decreases at higher CO_2 concentration in the gas phase. Moreover, the trend with respect to the total pressure is also the opposite between ideal and multicomponent diffusivity-selectivity. The fact that the calculated multicomponent diffusivity-selectivity decreases slightly with CO_2 fraction in the gas mixture, indicates that the reason for the poor size-selective behavior of the membrane in the multicomponent case lies in the CO_2-induced swelling of the membrane, that enhances CH_4 diffusion in the mixed gas case. This effect would be missed by an ideal evaluation of diffusivity.

The overall result predicted by the model is lower perm-selectivity compared to the pure gas case, as shown in Fig. 13e and f. Perm-selectivity shows the combination of solubility and diffusivity effects and the curves of ideal and multicomponent results cross. The perm-selectivity of an equimolar mixture of CO_2/CH_4 in CTA was validated against experimental data available, as seen in Section 4.1.4.

The relative weight of multicomponent effects on solubility-selectivity, diffusivity-selectivity and perm-selectivity can be assessed by reporting the ratio of multicomponent selectivity to ideal selectivity for the above mentioned quantities at fixed fugacity (chemical potential) of both gases. In this way, the ratio of multicomponent to ideal solubility selectivity is calculated and compared at constant fugacity of each gas between pure and mixed gas conditions. The results of the comparison are shown in Fig. 14 and they allow to assess that, on a relative basis, the departure from the ideal behavior, or in other words the extent of multicomponent effects, is more marked for diffusivity than for solubility. This indicates that, for cellulose acetates, swelling effects, which cause a reduction in diffusivity-selectivity, are more significant than

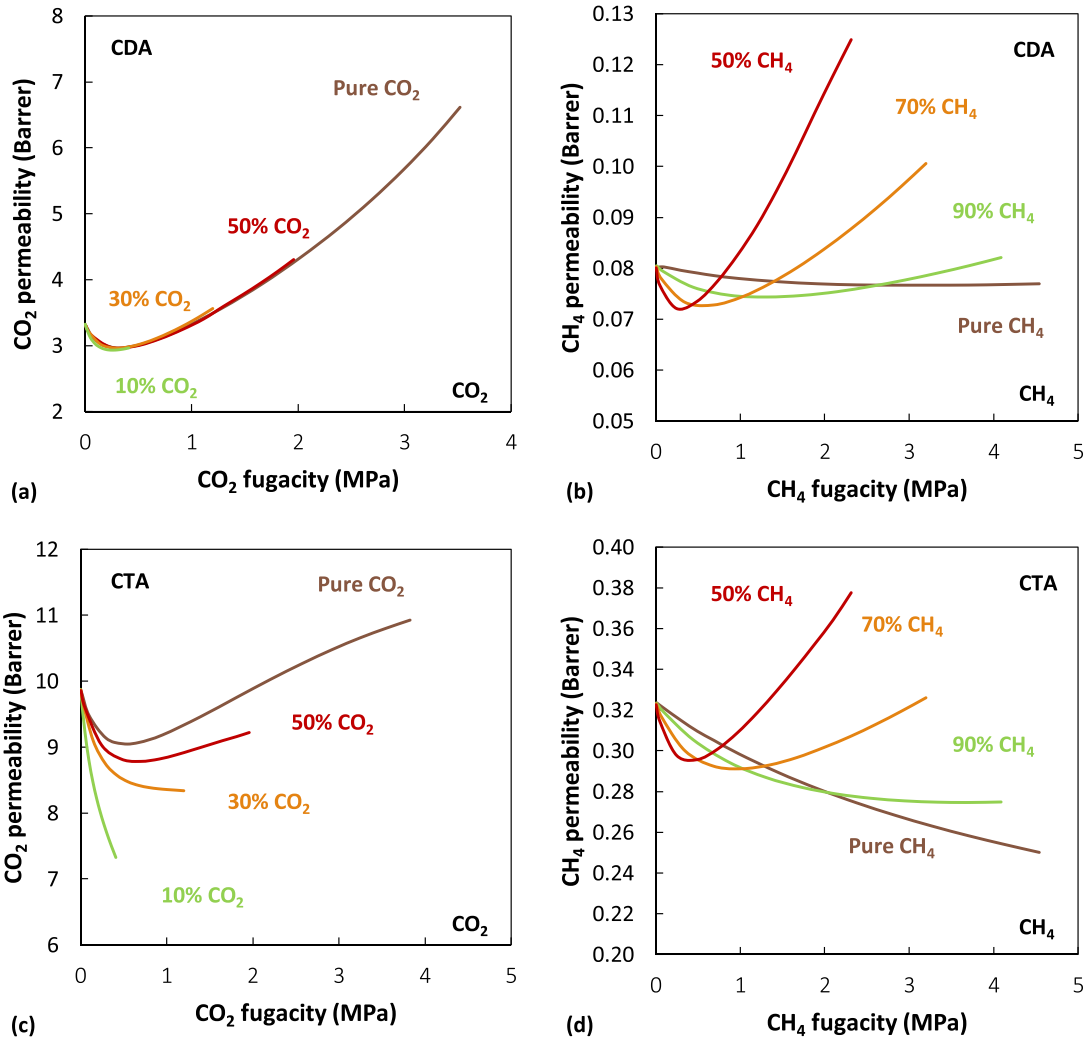

Fig. 12. Mixed gas permeation of 10/90 (green), 30/70 (orange) and 50/50 (red) mol% CO_2/CH_4 mixtures in CDA and CTA at 35 °C calculated with the ST model. The brown lines represent pure gas permeability. (For interpretation of the references to color in this figure legend, the reader is referred to the Web version of this article.)

competitive sorption, which enhances the solubility-selectivity.

Competition effects enhance the solubility-selectivity up to a factor of 2.2 and, the higher the CO_2 content in the gas mixture, the higher the enhancement. The effect also increases with pressure but flattens out at high pressures. By comparing the values of the two different materials, it can be seen that the enhancement of solubility-selectivity is stronger in CDA than in CTA. As a consequence, even though CDA has a lower ideal solubility-selectivity than CTA, at multicomponent conditions the situation reverses.

The behavior of diffusivity is opposite. First of all, the multicomponent value is significantly lower than the ideal one, and secondly the ratio between the two values decreases with pressure, but without reaching a plateau in the pressure range inspected. The multicomponent effect, that we believe to be associated to CO_2-induced swelling, increases with CO_2 fraction in the mixture. A comparison between the two polymers indicates that the reduction in diffusivity-selectivity associated with CO_2 induced swelling is stronger for CDA compared to CTA. This result is consistent with the fact that the parameter associated to the effect of swelling on diffusivity in the ST model, β, is higher for CDA than for CTA (10.5 *vs.* 5).

It is also interesting to notice that, in the low pressure range the perm-selectivity is slightly enhanced compared to the ideal value, and increases at increasing CO_2 content, due to the predominance of competitive sorption effects. However, the net increase is less than 10% for both materials. At higher pressure the trend is reversed and increasing the CO_2 content causes the perm-selectivity to drop. The effect is more marked in the case of CDA, compared to CTA, with maximum decrease of the perm-selectivity compared to ideal values of 40% and 30% respectively. The departure of perm-selectivity from the ideal behavior shown in Fig. 14 is calculated as the ratio of ideal and multicomponent perm-selectivity values, which were shown in Fig. 13, at the same pressure. The presence of a maximum and the crossing of the curves at different composition result from the combination of the two opposite trends of the underlying solubility and diffusivity contributions to permeability, namely α_S/α_{S0} that is monotonously increasing with pressure and with the amount of CO_2 present in the mixture, while α_D/α_{D0} is monotonously decreasing with it. As can be seen in Fig. 14, the average values calculated for α_S are approximately 16.2 for CTA and 19.6 for CDA, while for α_D they are 1.8 for CTA and 2.0 for CDA. Therefore, mixed-gas solubility-selectivity is approximately 10 times higher than diffusivity selectivity, thus being the main factor contributing to the multicomponent perm-selectivity. The pressure and composition dependence of perm-selectivity in the low pressure range follows the sorption behavior (competition), while the high pressure one

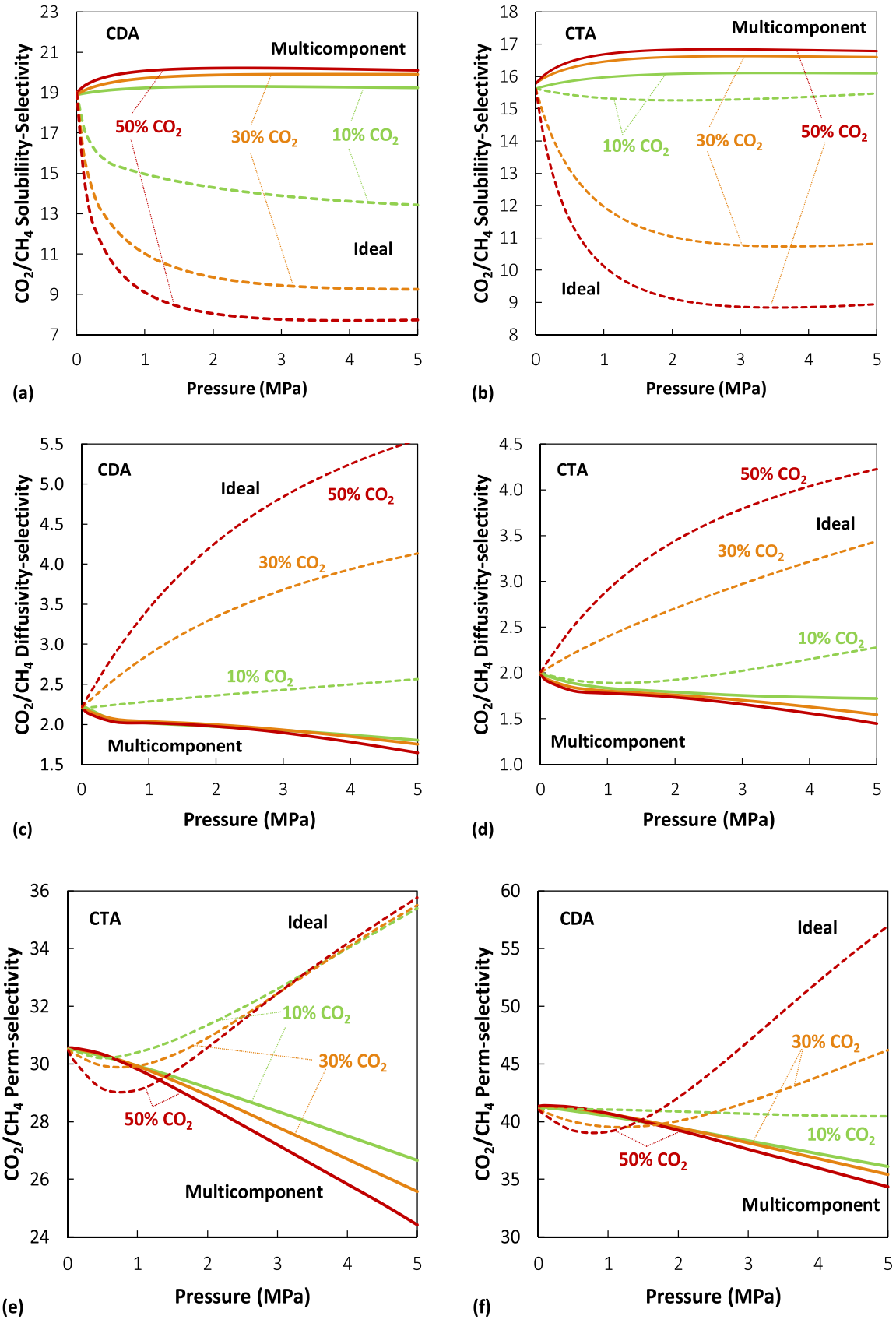

Fig. 13. CO_2/CH_4 solubility-selectivity, diffusivity-selectivity and perm-selectivity in CDA and CTA calculated with the NELF and ST models at 35 °C and at different mixture compositions: 10/90 mol% in green, 30/70 mol% in orange, 50/50 mol% in red. Dashed lines represent the ideal solubility-selectivity calculated with pure gas data. (For interpretation of the references to color in this figure legend, the reader is referred to the Web version of this article.)

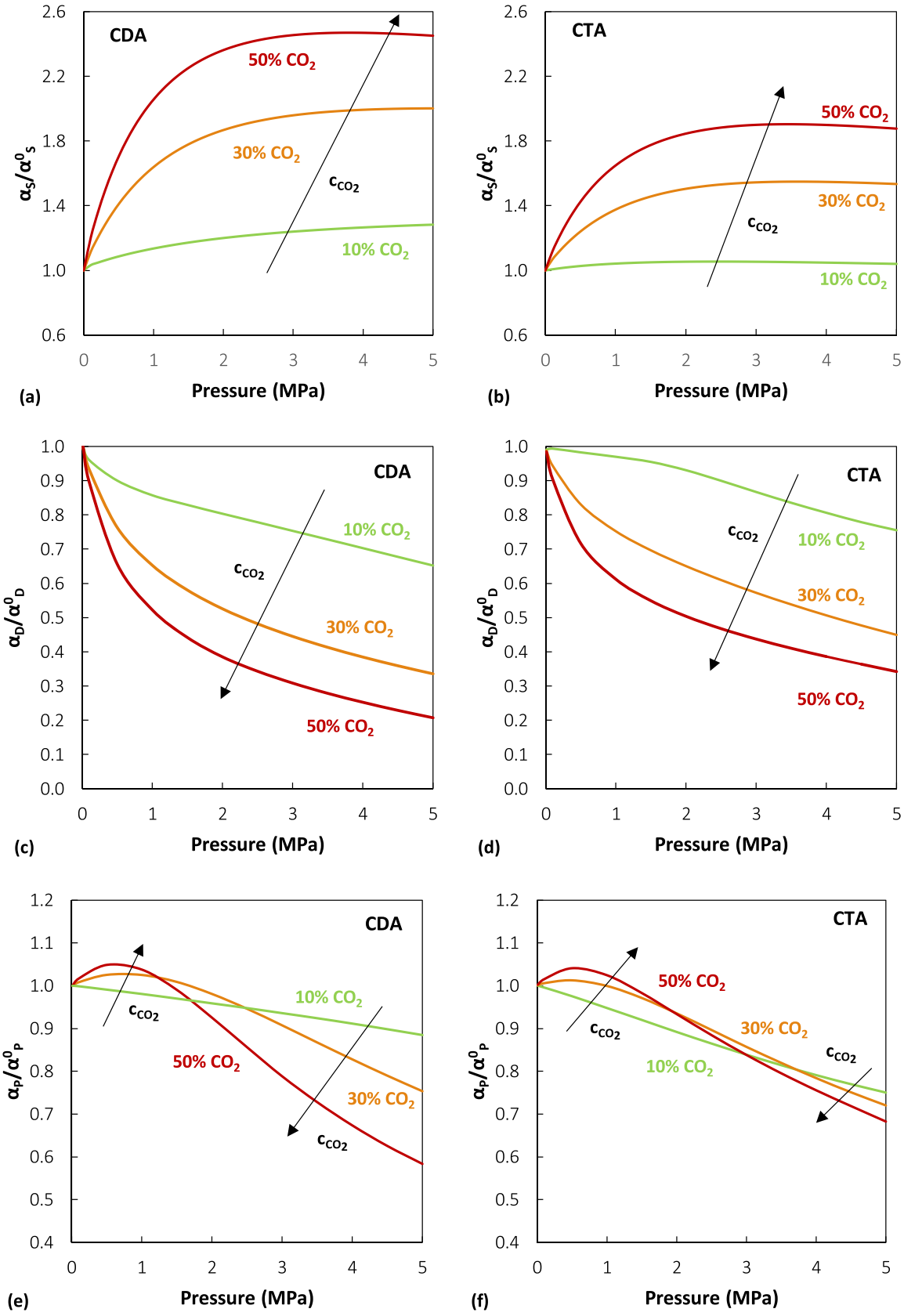

Fig. 14. Ratio of ideal and multicomponent CO_2/CH_4 solubility-selectivity, diffusivity-selectivity and perm-selectivity in CDA and CTA calculated with the NELF and ST models at 35 °C and at different mixture compositions: 10/90 mol% in green, 30/70 mol% in orange, 50/50 mol% in red. The arrows point in the direction of increasing CO_2 content in the gas phase. Ratios performed taking values of pure and mixed gas properties at the same gas fugacity value. (For interpretation of the references to color in this figure legend, the reader is referred to the Web version of this article.)

becomes controlled by diffusion (swelling), therefore, the dominating factor will depend on the operating conditions.

5. Conclusions

In this work a systematic modelling strategy for the study of multicomponent gas separation behavior of membranes was presented. The NELF model for gas sorption and the ST model for gas permeation were applied to analyze the gas transport properties of semicrystalline cellulose diacetate and triacetate, which are among the leading standard membrane materials for natural gas treatment.

The NELF model parameters, not previously available for cellulose acetates, were obtained via pressure-volume-temperature (*PVT*) data measured in this work. Furthermore, calorimetric tests were performed to quantify the crystalline fraction of the samples, which is assumed by the model to not contribute to gas sorption. Pure gas sorption measurements performed here and permeation data from the literature were used to obtain the binary energetic and swelling parameters of the NELF model and the mobility and plasticization factors of the ST model respectively. The approach was thoroughly validated against mixed gas sorption and permeation data from the literature, demonstrating good transferability of the pure polymer parameters obtained. In particular, the NELF model correctly represents the effect of temperature on sorption and predicts accurately the multicomponent CO_2/CH_4 sorption in CTA. Strong competitive exclusion of CH_4 from the membrane is observed when CO_2 is present, which enhances the solubility-selectivity. The ST model predictions of lower-than-ideal CO_2/CH_4 perm-selectivity for CTA are in agreement with the experimental evidence.

The model was then employed to carry out a predictive simulation of sorption, diffusion, and permeation at multicomponent conditions. This analysis provided indications of the strength of competitive sorption effects at different mixture compositions and different degrees of substitution of the materials: CDA exhibited higher values of the solubility-selectivity at multicomponent conditions and a higher enhancement of the solubility-selectivity as a result of competitive sorption compared to CTA. By assessing the mixed gas diffusion behavior, it was found that CO_2-induced swelling causes a faster diffusion of CH_4 in the mixed gas case. CTA is found to be less susceptible to the detrimental effects of CO_2-induced swelling, which cause a reduction of the diffusivity-selectivity. CTA perm-selectivity also displays a weaker dependence on the CO_2 content in the mixture.

Pure gas permeability and solubility data are readily available in the literature and allow the necessary model parameters to be obtained to carry out multicomponent calculations. In this regard, the proposed modelling strategy allows a comprehensive assessment of the material performance to be conducted and a fundamental analysis of the separation mechanism at multicomponent conditions. It represents an appealing strategy to extract additional information about multicomponent behavior, that is more relevant to the process, from already existing data or readily obtainable pure gas measurements.

CRediT author statement

Eleonora Ricci: Formal Analysis, Software, Visualization, Writing - Original Draft. **Ernesto Di Maio**: Investigation – *PVT* tests, Writing - Review and Editing. **Micaela Degli Esposti**: Investigation – calorimetric tests, Writing - Review and Editing. **Liang Liu**: Investigation – sorption tests, Writing - Review and Editing. **Giuseppe Mensitieri**: Resources, Writing - Review and Editing, Supervision. **Paola Fabbri**: Resources, Writing - Review and Editing, Supervision. **Sandra E. Kentish**: Resources, Writing - Review and Editing, Supervision. **Maria Grazia De Angelis**: Conceptualization, Resources, Writing - Review and Editing, Supervision.

Declaration of competing interest

The authors declare that they have no known competing financial interests or personal relationships that could have appeared to influence the work reported in this paper.

Acknowledgements

We are grateful to Francesco M. Benedetti, for his assistance in the preparation of thick cellulose acetate samples and in performing calorimetric tests.

Appendix A

Definition of symbols and parameters used in the SL and NELF models.

n_c	Number of components (gases + polymer)	
M_i	Molar mass of component i	
ρ_i	Density of component i	
v_i^*	Molar volume of a lattice cell of component i	
r_i^0	Number of lattice cells occupied by a molecule of pure component i	
ε_i	Non-bonded interaction energy between two lattice cells occupied by component i	
T_i^*	Characteristic temperature of component i	$T_i^* = \frac{\varepsilon_i}{k_b}$
p_i^*	Characteristic pressure of component i	$p_i^* = \frac{\varepsilon_i}{v_i^*}$
ρ_i^*	Characteristic density of component i	$\rho_i^* = \frac{M_i}{r_i v_i^*}$
$\widetilde{T}_i$	Reduced temperature of component i	$\widetilde{T}_i = \frac{T}{T_i^*}$
$\widetilde{p}_i$	Reduced pressure of component i	$\widetilde{p}_i = \frac{p}{p_i^*}$
$\widetilde{\rho}_i$	Reduced density of component i	$\widetilde{\rho}_i = \frac{\rho_i}{\rho_i^*}$
ρ	Density of the mixture	
k_{ij}	Binary interaction parameter between i and j	
ω_i	Mass fraction of component i	
φ_i	Volume fraction of component i in closed packed conditions	$\varphi_i = \frac{\omega_i/\rho_i^*}{\sum_i^N \omega_i/\rho_i^*}$

(*continued on next page*)

(*continued*)

ρ^*	Characteristic density of the mixture	$\frac{1}{\rho^*} = \sum_i^{n_c} \frac{\omega_i}{\rho_i^*}$
p^*	Characteristic pressure of the mixture	$p^* = \sum_i^{n_c} \varphi_i p_i^* - \sum_i^{n_c-1} \sum_{j>i}^{n_c} \varphi_i \varphi_j \Delta p_{ij}^*$ $\Delta p_{ij}^* = p_i^* + p_j^* - 2(1 - k_{ij}) \sqrt{p_i^* \cdot p_j^*}$
T^*	Characteristic temperature of the mixture	$T^* = \frac{p^*}{\sum_i^N \frac{p_i^* \varphi_i}{T_i^*}}$
v^*	Average close-packed molar volume in the mixture	$v^* = \frac{T^* R}{p^*}$
r_i	Number of lattice cells occupied by a molecule in mixture	$r_i = \frac{r_i^0 v_i^*}{v^*}$
$\widetilde{T}$	Reduced temperature of the mixture	$\widetilde{T} = \frac{T}{T^*}$
$\widetilde{p}$	Reduced pressure of the mixture	$\widetilde{p} = \frac{p}{p^*}$
$\widetilde{\rho}$	Reduced density of the mixture	$\widetilde{\rho} = \frac{\rho}{\rho^*}$

Appendix B. Supplementary data

Supplementary data to this article can be found online at https://doi.org/10.1016/j.memsci.2021.119226.

References

[1] O. Vopička, M.G. De Angelis, G.C. Sarti, Mixed gas sorption in glassy polymeric membranes: I. CO2/CH4 and n-C4/CH4 mixtures sorption in poly(1-trimethylsilyl-1-propyne) (PTMSP), J. Membr. Sci. 449 (2014) 97–108, https://doi.org/10.1016/j.memsci.2013.06.065.

[2] O. Vopička, M.G. De Angelis, N. Du, N. Li, M.D. Guiver, G.C. Sarti, Mixed gas sorption in glassy polymeric membranes: II. CO2/CH4 mixtures in a polymer of intrinsic microporosity (PIM-1), J. Membr. Sci. 459 (2014) 264–276, https://doi.org/10.1016/j.memsci.2014.02.003.

[3] W.J. Koros, E.S. Sanders, Multicomponent gas sorption in glassy polymers, J. Polym. Sci., Polym. Symp. (1985) 141–149, https://doi.org/10.1002/polc.5070720119.

[4] S.R. Reijerkerk, K. Nijmeijer, C.P. Ribeiro, B.D. Freeman, M. Wessling, On the effects of plasticization in CO2/light gas separation using polymeric solubility selective membranes, J. Membr. Sci. 367 (2011) 33–44, https://doi.org/10.1016/j.memsci.2010.10.035.

[5] G. Genduso, I. Pinnau, Quantification of sorption, diffusion, and plasticization properties of cellulose triacetate films under mixed-gas CO2/CH4 environment, J. Membr. Sci. 610 (2020), 118269, https://doi.org/10.1016/j.memsci.2020.118269.

[6] E.S. Sanders, W.J. Koros, H.B. Hopfenberg, V.T. Stannett, Mixed gas sorption in glassy polymers: equipment design considerations and preliminary results, J. Membr. Sci. 13 (1983) 161–174, https://doi.org/10.1016/S0376-7388(00)80159-3.

[7] A.E. Gemeda, M.G. De Angelis, N. Du, N. Li, M.D. Guiver, G.C. Sarti, Mixed gas sorption in glassy polymeric membranes. III. CO2/CH4 mixtures in a polymer of intrinsic microporosity (PIM-1): effect of temperature, J. Membr. Sci. 524 (2017) 746–757, https://doi.org/10.1016/j.memsci.2016.11.053.

[8] E. Ricci, A.E. Gemeda, N. Du, N. Li, M.G. De Angelis, M.D. Guiver, G.C. Sarti, Sorption of CO2/CH4 mixtures in TZ-PIM, PIM-1 and PTMSP: experimental data and NELF-model analysis of competitive sorption and selectivity in mixed gases, J. Membr. Sci. 585 (2019) 136–149, https://doi.org/10.1016/j.memsci.2019.05.026.

[9] G. Genduso, B.S. Ghanem, I. Pinnau, Experimental mixed-gas permeability, sorption and diffusion of CO2-CH4 mixtures in 6FDA-mPDA polyimide membrane: unveiling the effect of competitive sorption on permeability selectivity, Membranes (Basel) 9 (2019) 10, https://doi.org/10.3390/membranes9010010.

[10] G. Genduso, Y. Wang, B.S. Ghanem, I. Pinnau, Permeation, sorption, and diffusion of CO2-CH4 mixtures in polymers of intrinsic microporosity: the effect of intrachain rigidity on plasticization resistance, J. Membr. Sci. 584 (2019) 100–109, https://doi.org/10.1016/j.memsci.2019.05.014.

[11] H.D. Kamaruddin, W.J. Koros, Some observations about the application of Fick's first law for membrane separation of multicomponent mixtures, J. Membr. Sci. 135 (1997) 147–159, https://doi.org/10.1016/S0376-7388(97)00142-7.

[12] B.J. Story, W.J. Koros, Sorption and transport of CO2 and CH4 in chemically modified poly (phenylene oxide), J. Membr. Sci. 67 (1992) 191–210.

[13] E. Ricci, F.M. Benedetti, M.E. Dose, M.G. De Angelis, B.D. Freeman, D.R. Paul, Competitive sorption in CO2/CH4 separations: the case of HAB-6FDA polyimide and its TR derivative and a general analysis of its impact on the selectivity of glassy polymers at multicomponent conditions, J. Membr. Sci. 612 (2020) 118374, https://doi.org/10.1016/j.memsci.2020.118374.

[14] B.J. Story, W.J. Koros, Sorption of CO2/CH4 mixtures in poly(phenylene oxide) and a carboxylated derivative, J. Appl. Polym. Sci. 42 (1991) 2613–2626, https://doi.org/10.1002/app.1991.070420926.

[15] M. Galizia, W.S. Chi, Z.P. Smith, T.C. Merkel, R.W. Baker, B.D. Freeman, 50th anniversary perspective: polymers and mixed matrix membranes for gas and vapor separation: a review and prospective opportunities, Macromolecules 50 (2017) 7809–7843, https://doi.org/10.1021/acs.macromol.7b01718.

[16] S. Loeb, S. Sourirajan, Sea water demineralization by means of an osmotic membrane, in: Saline Water Conversion—II, American Chemical Society, 1963, pp. 117–132, https://doi.org/10.1021/ba-1963-0038.ch009.

[17] S. Liu, L.F. Hu, W.C. Zhang, H.Y. Ma, Cellulose acetate reverse osmosis membranes for desalination: a short review, Non-Metallic Mater. Sci. 1 (2019) 15–25, https://doi.org/10.30564/omms.v1i2.1143.

[18] C.A. Scholes, G.W. Stevens, S.E. Kentish, Membrane gas separation applications in natural gas processing, Fuel 96 (2012) 15–28, https://doi.org/10.1016/j.fuel.2011.12.074.

[19] J.K. Adewole, A.L. Ahmad, S. Ismail, C.P. Leo, Current challenges in membrane separation of CO2 from natural gas: a review, Int. J. Greenh. Gas Control. 17 (2013) 46–65, https://doi.org/10.1016/j.ijggc.2013.04.012.

[20] R.W. Baker, K. Lokhandwala, Natural gas processing with membranes: an overview, Ind. Eng. Chem. Res. 47 (2008) 2109–2121, https://doi.org/10.1021/ie071083w.

[21] G.S. Cerveira, C.P. Borges, F. de A. Kronemberger, Gas permeation applied to biogas upgrading using cellulose acetate and polydimethylsiloxane membranes, J. Clean. Prod. 187 (2018) 830–838, https://doi.org/10.1016/j.jclepro.2018.03.008.

[22] H.T. Lu, S. Kanehashi, C.A. Scholes, S.E. Kentish, The potential for use of cellulose triacetate membranes in post combustion capture, Int. J. Greenh. Gas Control 555 (2016) 362–368, https://doi.org/10.1016/j.memsci.2018.03.045.

[23] P. Zugenmaier, 4. Characteristics of cellulose acetates— 4.1 Characterization and physical properties of cellulose acetates, Macromol. Symp. 208 (2004) 81–166, https://doi.org/10.1002/masy.200450407.

[24] A.C. Puleo, D.R. Paul, S.S. Kelley, The effect of degree of acetylation on gas sorption and transport behaviour in cellulose acetate, J. Membr. Sci. 47 (1989) 301–332.

[25] K. Kamide, M. Saito, Thermal analysis of cellulose acetate solids with total degrees of substitution of 0.49, 1.75, 2.46, and 2.92, Polym. J. 17 (1985) 919–928, https://doi.org/10.1295/polymj.17.919.

[26] N. Choji, W. Pusch, M. Satoh, T.-M. Tak, A. Tanioka, Structure investigations of homogeneous cellulose acetate membranes by gas permeation measurements, Desalination 53 (1985) 347–361, https://doi.org/10.1016/0011-9164(85)85072-4.

[27] M. Saberi, A.A. Dadkhah, S.A. Hashemifard, Modeling of simultaneous competitive mixed gas permeation and CO2 induced plasticization in glassy polymers, J. Membr. Sci. 499 (2016) 164–171, https://doi.org/10.1016/j.memsci.2015.09.044.

[28] M. Saberi, S.A. Hashemifard, A.A. Dadkhah, Modeling of CO2/CH4 gas mixture permeation and CO2 induced plasticization through asymmetric cellulose acetate membrane, RSC Adv. 6 (2016) 16561–16567, https://doi.org/10.1039/C5RA23506E.

[29] E. Magnanelli, Ø. Wilhelmsen, E. Johannessen, S. Kjelstrup, Enhancing the understanding of heat and mass transport through a cellulose acetate membrane for CO2 separation, J. Membr. Sci. 513 (2016) 129–139, https://doi.org/10.1016/j.memsci.2016.04.021.

[30] J. Guo, T.A. Barbari, Unified dual mode description of small molecule sorption and desorption kinetics in a glassy polymer, Macromolecules 42 (2009) 5700–5708, https://doi.org/10.1021/ma9007576.

[31] J. Guo, T.A. Barbari, A dual mode, local equilibrium relaxation model for small molecule diffusion in a glassy polymer, Macromolecules 41 (2008) 238–245, https://doi.org/10.1021/ma071662c.

[32] L. Perrin, Q.T. Nguyen, D. Sacco, P. Lochon, Experimental studies and modelling of sorption and diffusion of water and alcohols in cellulose acetate, Polym. Int. 42 (1997) 9–16, https://doi.org/10.1002/(SICI)1097-0126(199701)42:1<9::AID-PI637>3.0.CO;2-A.

[33] E. Ricci, M.G. De Angelis, Modelling mixed-gas sorption in glassy polymers for CO2 removal: a sensitivity analysis of the dual mode sorption model, Membranes (Basel) 9 (2019) 8, https://doi.org/10.3390/membranes9010008.

[34] F. Doghieri, G.C. Sarti, Nonequilibrium lattice fluids: a predictive model for the solubility in glassy polymers, Macromolecules 29 (1996) 7885–7896, https://doi.org/10.1021/ma951366c.

[35] M. Minelli, G.C. Sarti, Permeability and diffusivity of CO2 in glassy polymers with and without plasticization, J. Membr. Sci. 435 (2013) 176–185, https://doi.org/10.1016/j.memsci.2013.02.013.

[36] J.G. Wijmans, R.W. Baker, The solution-diffusion model: a review, J. Membr. Sci. 107 (1995) 1–21, https://doi.org/10.1016/S0166-4115(08)60038-2.

[37] E. Toni, M. Minelli, G.C. Sarti, A predictive model for the permeability of gas mixtures in glassy polymers, Fluid Phase Equil. 455 (2018) 54–62, https://doi.org/10.1016/j.fluid.2017.09.025.

[38] D. Peng, D.B. Robinson, A new two-constant equation of state, Ind. Eng. Chem. Fundam. 15 (1976) 59–64, https://doi.org/10.1021/i160057a011.

[39] S.I. Sandler, Chemical, Biochemical, and Engineering Thermodynamics, fifth ed., John Wiley & Sons, Hoboken, NJ, USA, 2017.

[40] F. Doghieri, M. Quinzi, D.G. Rethwisch, G.C. Sarti, Predicting gas solubility in glassy polymers through nonequilibrium EOS. Adv. Mater. Membr. Sep., American Chemical Society, Washington, DC, USA, 2004, pp. 74–90, https://doi.org/10.1021/bk-2004-0876.ch005.

[41] G.C. Sarti, F. Doghieri, Predictions of the solubility of gases in glassy polymers based on the NELF model, Chem. Eng. Sci. 53 (1998) 3435–3447, https://doi.org/10.1016/S0009-2509(98)00143-2.

[42] I.C. Sanchez, R.H. Lacombe, Statistical thermodynamics of polymer solutions, Macomolecules 11 (1978) 1145–1156. http://pubs.acs.org/doi/pdf/10.1021/ma60066a017. (Accessed 26 June 2017).

[43] R.H. Lacombe, I.C. Sanchez, Statistical thermodynamics of fluid mixtures, J. Phys. Chem. 80 (1976) 2568–2580, https://doi.org/10.1021/j100564a009.

[44] M.G. De Angelis, G.C. Sarti, Solubility of gases and liquids in glassy polymers, Annu. Rev. Chem. Biomol. Eng. 2 (2011) 97–120, https://doi.org/10.1146/annurev-chembioeng-061010-114247.

[45] B. Bonavoglia, G. Storti, M. Morbidelli, Modeling of the sorption and swelling behavior of semicrystalline polymers in supercritical CO2, Ind. Eng. Chem. Res. 45 (2006) 1183–1200, https://doi.org/10.1021/ie050842c.

[46] M. Minelli, M.G.M.G. De Angelis, An equation of state (EoS) based model for the fluid solubility in semicrystalline polymers, Fluid Phase Equil. 367 (2014) 173–181, https://doi.org/10.1016/j.fluid.2014.01.024.

[47] M. Fischlschweiger, A. Danzer, S. Enders, Predicting gas solubility in semi-crystalline polymer solvent systems by consistent coupling of Sanchez-Lacombe EOS with a continuum mechanics approach, Fluid Phase Equil. 506 (2020) 112379, https://doi.org/10.1016/j.fluid.2019.112379.

[48] L. Onsager, Theories and problems of liquid diffusion, Ann. N. Y. Acad. Sci. 46 (1945) 241–265.

[49] C. Truesdell, Mechanical basis of diffusion, J. Chem. Phys. 37 (1962) 2336–2344, https://doi.org/10.1063/1.1733007.

[50] R.J. Bearman, J.G. Kirkwood, M. Fixman, Statistical-mechanical theory of transport processes. X. The heat of transport in binary liquid solutions, Adv. Chem. Phys. 1 (1958) 1–13.

[51] R.B. Bird, D.J. Klingenberg, Multicomponent diffusion-A brief review, Adv. Water Resour. 62 (2013) 238–242, https://doi.org/10.1016/j.advwatres.2013.05.010.

[52] M. Minelli, G.C. Sarti, Gas permeability in glassy polymers: a thermodynamic approach, Fluid Phase Equil. 424 (2015) 44–51, https://doi.org/10.1016/j.fluid.2015.09.027.

[53] M. Minelli, G.C. Sarti, Elementary prediction of gas permeability in glassy polymers, J. Membr. Sci. 521 (2017) 73–83, https://doi.org/10.1016/j.memsci.2016.09.001.

[54] P. Zoller, P. Bolli, V. Pahud, H. Ackermann, Apparatus for measuring pressure–volume–temperature relationships of polymers to 350 °C and 2200 kg/cm2, Rev. Sci. Instrum. 47 (1976) 948–952.

[55] J.H. Dymond, R. Malhotra, The Tait Equation : 100 Years on, Int. J. Thermophys. 9 (1988) 941–951.

[56] Standard Test Methods for Density and Specific Gravity (Relative Density) of Plastics by Displacement, ASTM Int., West Conshohocken, 2013, https://doi.org/10.1520/D0792-13.

[57] N. Spanic, V. Jambrekovic, S. Medved, A. Antonovic, Chemical and thermal properties of cellulose acetate prepared from white willw (salix almba) and black alder (alnus glutinosa) as potential polymeric base of biocomposite materials, Chem. Biochem. Eng. Q. 29 (2015) 357–365, https://doi.org/10.15255/CABEQ.2015.2176.

[58] H.S. Barud, A.M. De Araújo Júnior, R.M.N. De Assunção, C.S. Meireles, D. A. Cerqueira, G.R. Filho, Y. Messaddeq, S.J.L. Ribeiro, Thermal characterization of cellulose acetate produced from homogeneous acetylation of bacterial cellulose, in: 9no Congr. Bras. Polym, 2007.

[59] D.A. Cerqueira, G.R. Filho, R.M.N. Assunção, G. Rodrigues Filho, R.M.N. Assunção, A new value for the heat of fusion of a perfect crystal of cellulose acetate, Polym. Bull. 56 (2006) 475–484, https://doi.org/10.1007/s00289-006-0511-9.

[60] H.S. Barud, A.M. De Ara, D.B. Santos, C.S. Meireles, D.A. Cerqueira, R.M.N. De Assunc, Thermal behavior of cellulose acetate produced from homogeneous acetylation of bacterial cellulose, Thermochim. Acta 471 (2008) 61–69, https://doi.org/10.1016/j.tca.2008.02.009.

[61] G.Q. Chen, S. Kanehashi, C.M. Doherty, A.J. Hill, S.E. Kentish, Water vapor permeation through cellulose acetate membranes and its impact upon membrane separation performance for natural gas purification, J. Membr. Sci. 487 (2015) 249–255, https://doi.org/10.1016/j.memsci.2015.03.074.

[62] L.-G. Tang, D.N.-S. Hon, Y.-Q. Zhu, Polymorphic transformations of cellulose acetates prepared by solution acetylation at an elevated temperature, J. Macromol. Sci. Part A. 33 (1996) 203–208, https://doi.org/10.1080/10601329608010863.

[63] A.J. Stipanovic, A. Sarko, I. The, Molecular and crystal structure of cellulose triacetate I: a parallel chain structure, Polymer (Guildf) 19 (1978) 3–8, https://doi.org/10.1016/0032-3861(78)90164-7.

[64] E. Roche, H. Chanzy, M. Boudeulle, R.H. Marchessault, P. Sundararajan, Three-Dimensional crystalline structure of cellulose triacetate II, Macromolecules 11 (1978) 86–94, https://doi.org/10.1021/ma60061a016.

[65] P. Sikorski, M. Wada, L. Heux, H. Shintani, B.T. Stokke, Crystal structure of cellulose triacetate I, Macromolecules 37 (2004) 4547–4553, https://doi.org/10.1021/ma0498520.

[66] H. Kono, Y. Numata, T. Erata, M. Takai, Structural analysis of cellulose triacetate polymorphs by two-dimensional solid-state 13C-13C and 1H-13C correlation NMR spectroscopies, Polymer (Guildf) 45 (2004) 2843–2852, https://doi.org/10.1016/j.polymer.2004.01.075.

[67] H. Kono, Y. Numata, N. Nagai, T. Erata, M. Takai, CPMAS13C NMR and X-ray studies of cellooligosaccharide acetates as a model for cellulose triacetate, J. Polym. Sci. Part A Polym. Chem. 37 (1999) 4100–4107, https://doi.org/10.1002/(SICI)1099-0518(19991115)37:22<4100::AID-POLA8>3.0.CO;2-D.

[68] H. Kono, T. Erata, M. Takai, CP/MAS 13 C NMR study of cellulose and cellulose derivatives. 2. Complete assignment of the 13 C resonance for the ring carbons of cellulose triacetate polymorphs, J. Am. Chem. Soc. 124 (2002) 7512–7518, https://doi.org/10.1021/ja010705g.

[69] Y. Numata, H. Kumagai, H. Kono, T. Erata, M. Takai, Structural analysis of cellulose triacetate I by molecular dynamics simulation, J. Fiber Sci. Technol. 60 (2004) 75–80, https://doi.org/10.2115/fiber.60.75.

[70] T. Kobayashi, D. Hayakawa, T. Khishigjargal, K. Ueda, Investigation of the structure and interaction of cellulose triacetate I crystal using ab initio calculations, Carbohydr. Res. 388 (2014) 61–66, https://doi.org/10.1016/j.carres.2014.02.015.

[71] J.L. Braun, J.F. Kadla, Cta III, A third polymorph of cellulose triacetate, J. Carbohydr. Chem. 32 (2013) 120–138, https://doi.org/10.1080/07328303.2012.752493.

[72] A.A. Hanna, A.H. Basta, H. El-saied, I.F. Abadir, Thermal properties of cellulose acetate and its complexes with some transition metals, Polym. Degrad. Stabil. 63 (1999) 293–296, https://doi.org/10.1016/S0141-3910(98)00108-6.

[73] O. Ishida, D.-Y. Kim, S. Kuga, Y. Nishiyama, R. Malcolm Brown Jr., Microfibrillar carbon from native cellulose, Cellulose 11 (2004) 475–480, https://doi.org/10.1023/B:CELL.0000046410.31007.0b.

[74] C.J. Malm, L.B. Genung, J.V. Fleckenstein, Densities of cellulose esters, Ind. Eng. Chem. 39 (1947) 1499–1504, https://doi.org/10.1021/ie50455a022.

[75] P. Zoller, D. Walsh, Standard Pressure–Volume–Temperature Data for Polymers, Technomic- Lancaster, 1995.

[76] M. Wada, R. Hori, X-ray diffraction study of the thermal expansion behavior of cellulose triacetate I, J. Polym. Sci. B. 47 (2009) 517–523, https://doi.org/10.1002/polb.

[77] A. Odajima, T. Maeda, Calculation of the elastic constants and the lattice energy of the polyethylene crystal, J. Polym. Sci. Part C Polym. Symp. 15 (1966) 55–74, https://doi.org/10.1002/polc.5070150106.

[78] T. Ito, H. Marui, Pressure–strain and pressure–volume relationships in the crystal lattice of polyethylene at 293°K, Polym. J. 2 (1971) 768–782, https://doi.org/10.1295/polymj.2.768.

[79] A. Bocahut, J.-Y. Delannoy, V. Caroll, K. Mazeau, Conformational Analysis of Cellulose Acetate in the Dense Amorphous State, 2014.

[80] W. Hu, J. Xie, H.W. Chau, B.C. Si, Evaluation of parameter uncertainties in nonlinear regression using Microsoft Excel Spreadsheet, Environ. Syst. Res. 4 (2015), https://doi.org/10.1186/s40068-015-0031-4.

[81] R. Swaidan, B. Ghanem, M. Al-Saeedi, E. Litwiller, I. Pinnau, Role of intrachain rigidity in the plasticization of intrinsically microporous triptycene-based polyimide membranes in mixed-Gas CO2/CH4 separations, Macromolecules 47 (2014) 7453–7462, https://doi.org/10.1021/ma501798v.

[82] A.Y. Houde, B. Krishnakumar, S.G. Charati, S.A. Stern, Permeability of dense (homogeneous) cellulose acetate membranes to methane, carbon dioxide, and their mixtures at elevated pressures, J. Appl. Polym. Sci. 62 (1996) 2181–2192, https://doi.org/10.1002/(SICI)1097-4628(19961226)62:13<2181::AID-APP1>3.0.CO;2-F.

[83] S.A. Stern, A.H. De Meringo, Solubility of carbon dioxide in cellulose acetate at elevated pressures, J. Polym. Sci., Part B: Polym. Phys. 16 (1978) 751.

[84] S.A. Stern, S.S. Kulkarni, Solubility of methane in cellulose acetate - conditioning effect of carbon dioxide, J. Membr. Sci. 10 (1982) 235–251.
[85] E. Ricci, M. Minelli, M.G. De Angelis, A multiscale approach to predict the mixed gas separation performance of glassy polymeric membranes for CO2 capture: the case of CO2/CH4 mixture in Matrimid®, J. Membr. Sci. 539 (2017) 88–100, https://doi.org/10.1016/j.memsci.2017.05.068.
[86] M. Minelli, B.R. Pimentel, M.L. Jue, R.P. Lively, G.C. Sarti, Analysis and utilization of cryogenic sorption isotherms for high free volume glassy polymers, Polymer (Guildf) 170 (2019) 157–167, https://doi.org/10.1016/j.polymer.2019.03.012.